



Geotechnical studies and primary support design for a highway tunnel: a case study in Turkey

Ayberk Kaya¹ · Fikri Bulut²

Received: 7 November 2018 / Accepted: 11 April 2019 / Published online: 4 May 2019
© Springer-Verlag GmbH Germany, part of Springer Nature 2019

Abstract

The main aim of this study is to appraise the geotechnical characteristic of the rock masses and to propose the proper support design for the Cankurtaran Tunnel project situated in NE Turkey. The exhaustive engineering geological investigations were done to determine the characteristic of rock masses that primarily consist of volcanic and sedimentary rocks. The tunnel route was divided into 15 segments according to their lithological and structural properties. The rock mass rating (RMR) and Rock Mass Quality Index (Q) systems were used to determine the quality of rock masses and final tunnel lining support. To check the capacity of the suggested support units analytically, the convergence-confinement (CC) technique was applied. The efficiency of the support design, dimensions of the plastic zones and deformations were determined using the 2D and 3D numerical finite element method (FEM) modeling. The empirical support system suggested in this study reduced the total displacement and dimension of the plastic zone.

Keywords Tunneling · Convergence-confinement method · Rock mass classification · FEM · Tunnel lining design

Introduction

Selection of the most economical and suitable support design contributes positively to an underground excavation project in design and construction processes. Empirical, analytical and numerical approaches are generally preferred methods when tunnels are projected by designers. In order to design tunnel supports, several researchers have suggested rock mass classification systems which have gained universal acceptance (i.e. Terzaghi 1946; Lauffer 1958; Rabcewicz 1964; Wickham et al. 1972; Barton et al. 1974; Bieniawski 1989; Palmström 1995; Marinos and Hoek 2000; Aydan et al. 2014). Due to their practicality, the Rock Mass Quality Index (Q; Barton et al. 1974) and rock mass rating (RMR; Bieniawski 1989) classifications are widely utilized

systems by many geotechnical engineers. In spite of the fact that these techniques are advantageous instruments in preliminary support design, they do not provide essential information in strain and stress estimations. Therefore, numerical methods gain popularity in determination of stress distributions and deformations, and checking the lining design for the best remedy. Recent research has showed that if empirical techniques are integrated into numerical methods, more realistic outcomes in lining design will be acquired (i.e. Basarir 2006; Gurocak et al. 2007; Sopaci and Akgun 2008; Kaya et al. 2011; Aydin et al. 2014; Yalcin et al. 2015; Lin et al. 2017; Kanik and Gurocak 2018).

The Turkish General Directorate of Highways (TGDH) planned a project for reclamation of the Artvin–Hopa motorway (km: 6 + 500 – 13 + 787) owing to increasing traffic load and congestion. This project includes construction of the double-tubed Cankurtaran Tunnel situated between km: 7 + 980 – 13 + 208. The total length of the modified horseshoe-shaped tunnel is 5.228 km, and the tunnel is constructed using mechanical excavation and conventional drilling-blasting techniques subjected to existing rock mass behaviors and conditions. The planned, unsupported span and height are 12 and 9 m, respectively. The height of surcharge ranges between 80

✉ Ayberk Kaya
ayberk.kaya@erdogan.edu.tr

¹ Faculty of Engineering, Department of Civil Engineering, Recep Tayyip Erdogan University, 53100 Rize, Turkey

² Faculty of Engineering, Department of Geological Engineering, Karadeniz Technical University, 61080 Trabzon, Turkey

and 410 m above the tunnel. The map showing the tunnel location is presented in Fig. 1, and the field view of the entrance and exit sections are given in Fig. 2a–b.

In the present study, the Cankurtaran Tunnel was selected as an implementation site for the empirical, analytical and numerical tunnel support process. A geotechnical

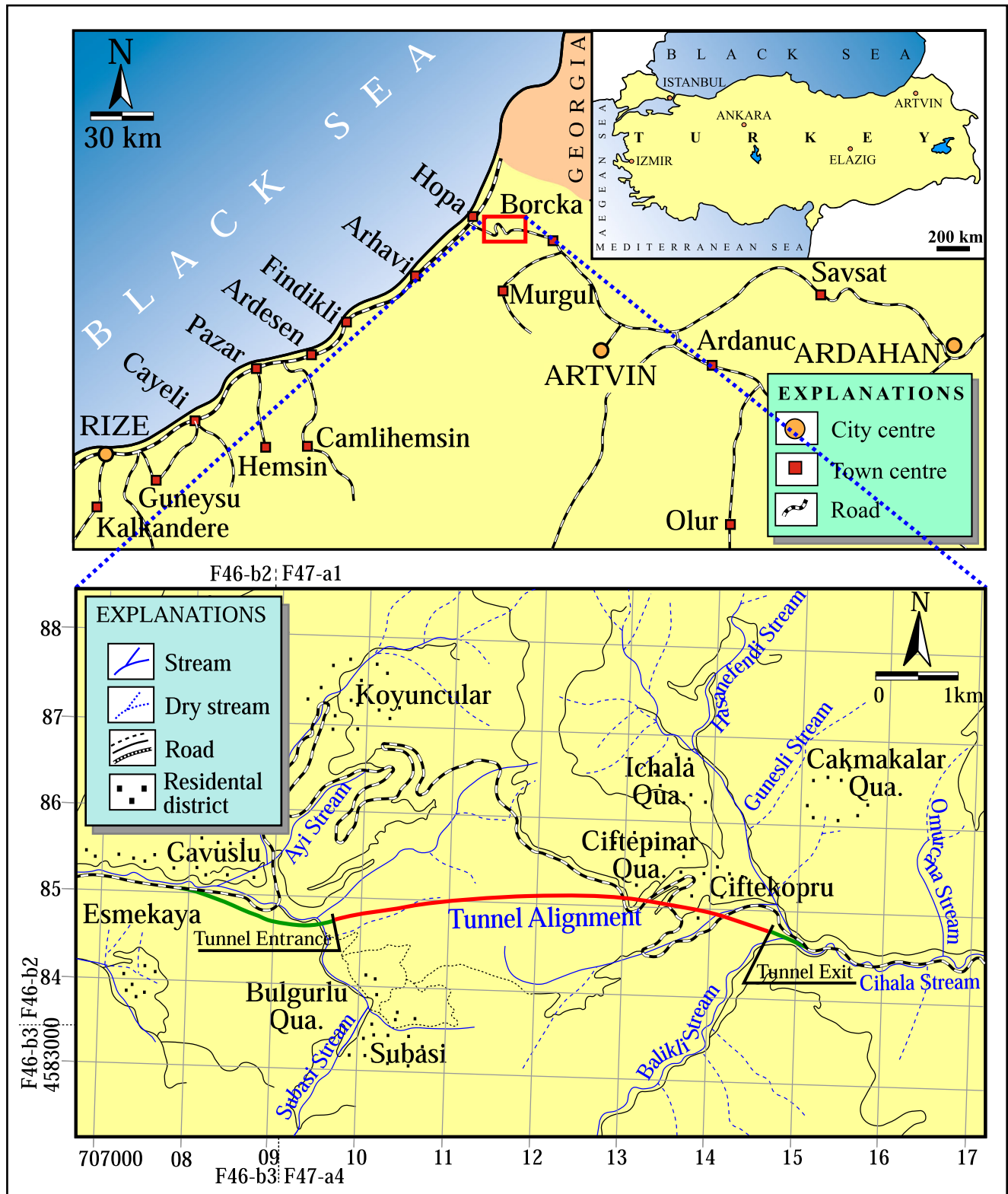
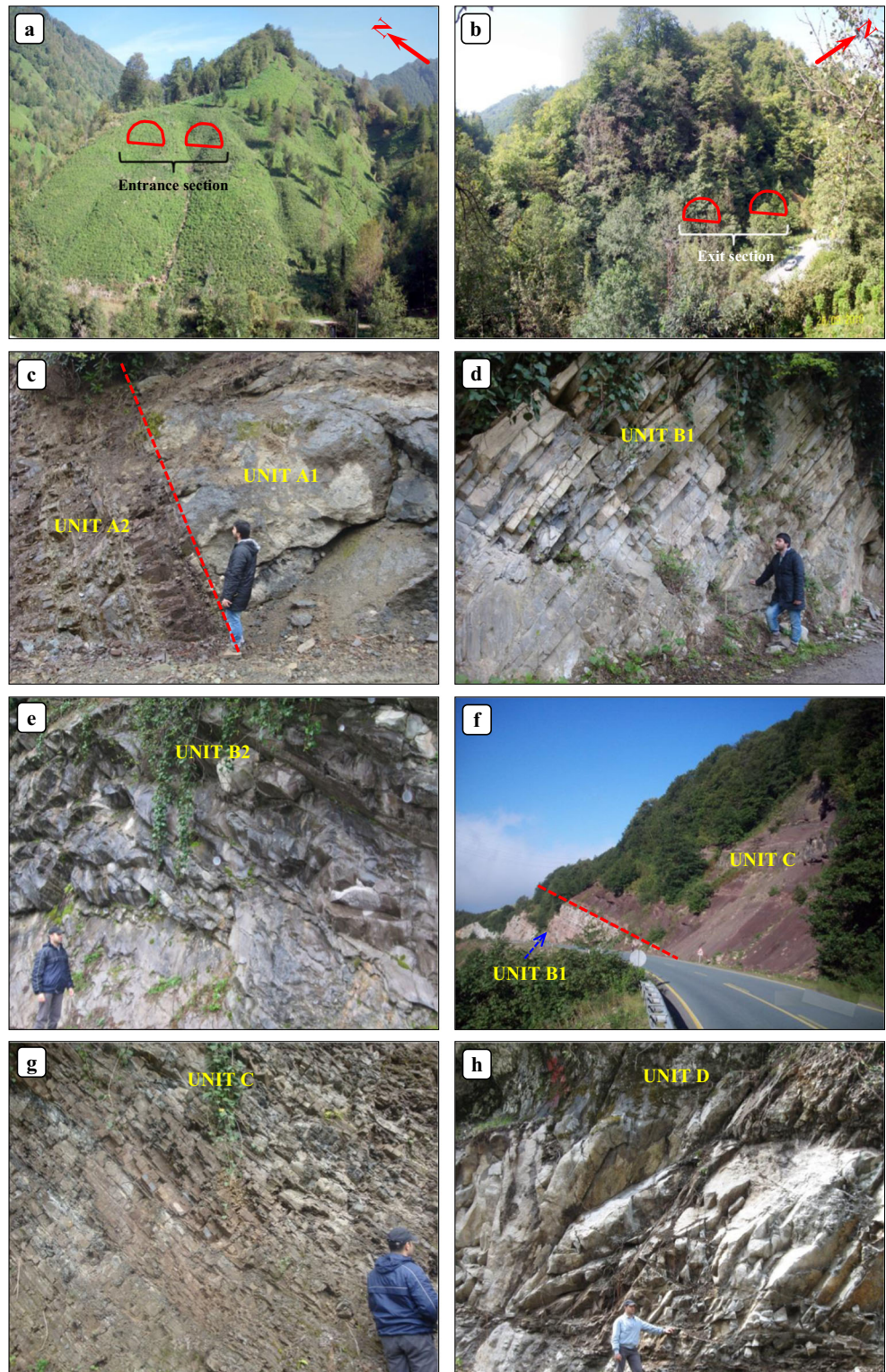


Fig. 1 Location map of the study area

Fig. 2 (a) Pre-excavation view of the entrance, (b) exit sections and field view of the (c) A1 and A2, (d) B1, (e) B2, (f, g) C and (h) D geotechnical units



investigation followed by rock mass classification and numerical modeling was carried out. The performance of empirical support design was also controlled via finite element method (FEM) modeling. In this framework, the 2D FEM results were compared against 3D analysis results and assessed.

Study area

Based on the structural and lithological arguments, the Eastern Pontide Tectonic Assembly is divided into northern and southern zones (Ketin 1966; Guven 1993). The ages of geological

units in the Eastern Pontide vary between Paleozoic and Cenozoic. The tunnel is located in the northern zone, and four formations crop out along the tunnel route (Capkinoglu 1981).

The Subasi Ridge Formation consists of andesitic pyroclastic rocks and intercalations of sandstone, limestone, marl and tuff (Fig. 2c). The Late Cretaceous-aged unit is generally located at the entrance section of the tunnel. The Late Cretaceous-Paleocene-aged Cankurtaran Formation cropped out in the inner section is defined by limestone and marl, and conformably overlies the Subasi Ridge Formation. While the lower and upper parts of the formation are thin-bedded (Fig. 2d), the middle part is thick-bedded (Fig. 2e). In the inner part of the tunnel, the Subasi and Cankurtaran Ridge Formations are juxtaposed along the NE–SW-trending inactive vertical faults F1 and F2. The Paleocene-aged Senkaya Ridge Formation is a sedimentary package including thin- to medium-layered marl and limestone with interbedded claystone (Fig. 2f and g). This unit is generally located towards the end of the inner part of the tunnel. The Eocene-aged Kabakoy Formation which is usually cropped out at the exit part of the tunnel consists of basalt-andesite and pyroclastic rocks (Fig. 2h), and unconformably overlies the Senkaya Ridge Formation. Near the village of Ciftekopru, the Senkaya Ridge and Kabakoy Formations are juxtaposed along the NE–SW-trending inactive vertical fault F3.

In this study, for convenience, the andesitic pyroclastites in the Subasi Ridge Formation were named as “unit A1” and as “unit A2” for sedimentary intercalations (Fig. 2c). The thin-bedded and thick-bedded levels of the Cankurtaran Formation were designated as “unit B1” and “unit B2”, respectively (Fig. 2d and e). Furthermore, the Senkaya Ridge Formation was symbolized as “unit C” and as “unit D” for the Kabakoy Formation (Fig. 2f–h). Figure 3 shows the generalized geological map of the study area. The rock masses in the portal sections and fault zones (F1, F2 and F3) were also delineated as separate segments in this study (Fig. 4).

The geological cross section was prepared by the help of the drilling, seismic survey and field studies data, and the tunnel route was divided into 15 segments based on the structural, lithological and geotechnical properties. The tunnel segments are shown in Fig. 4.

Method

Geotechnical studies

Geotechnical characteristic of the rock units located along the Cankurtaran Tunnel alignment were determined performing surface, subsurface and laboratory studies. The field work consisted of mapping, drilling, scan-line survey, water pressure test, seismic investigation and geotechnical description.

Because of the dense vegetation and steep morphology, seven drillings (total length of 607 m) have been opened under the control of the TGDH (Figs. 3 and 4) to monitor the ground properties at the tunnel depth, to characterize the joint features and groundwater level, core sampling, and water pressure tests (Lugeon test). Three of the drillings (BH 1–3) were placed at the inlet section, one borehole (BH 7) at the outlet part and another three (BH 4–6) towards the center of the tunnel line.

The water pressure tests suggested by Lugeon (1933) were performed to identify the permeability properties of the tunnel ground and, therefore, to collect data on the water inflow potency into the tunnel. Along the tunnel alignment, the groundwater depth varied between 3.4 and 17.6 m. The Lugeon tests were carried out below the groundwater level in all boreholes at 5-m intervals. The Lugeon experiment results showed that the rock mass permeability varied from very low to moderate for “unit A1 [0.92–5.74 Lugeon units (Lu)]” and “unit A2 (0.38–6.72 Lu)” considering the classification suggested by Quinones-Rozo (2010). On the other hand, the permeability of rock mass varied from very low to low for “unit B1 (0.00–1.08 Lu)” and “unit B2 (0.32–4.17 Lu).” However, the permeability of rock mass is very low (0.00–0.32 Lu) for “unit C” and low (1.02–5.00 Lu) for “unit D.”

In other words, based on the average Lugeon values of the rock masses presented in Table 1, unit A1, unit A2, unit B2 and unit D exhibit low permeability, and unit B1 and unit C are impermeable considering the classification of Lugeon (1933). A general decrease in permeability with depth was observed due to the reduction in fracture aperture and filling of joints with clay particles during weathering. These data indicate that the geotechnical units are generally dry, and no sudden water flows were expected during the tunnel excavation. On the other hand, because the fault zone materials located along the tunnel consist of finer grain size and angular shape of fractured grains, these zones were assumed to be more permeable than non-faulted rock masses. Therefore, difficulties due to the risk of sudden water flow are possible during the excavation of fault zones.

Laboratory experiments were performed on the core samples compiled from the drillings and rock blocks based on the techniques suggested by ISRM (2007) to define the physical, mechanical and elastic characteristics of the intact rocks, including unit weight (γ), uniaxial compressive strength (σ_{ci}), point load strength index ($I_{S(50)}$), and Young’s modulus (E_i). In addition to this, the rock quality designation (RQD) was defined from drillings and scan-line surveys using the methods proposed by Deere (1964) and Priest and Hudson (1976). The average RQD values and rock quantities for the geotechnical unit A1, unit A2, unit B1, unit B2, unit C and unit D were found to be 84% good, 60% fair, 62% fair, 88% good, 3% very poor and 73% fair, respectively. Table 1 demonstrates the results of laboratory test and RQD values.

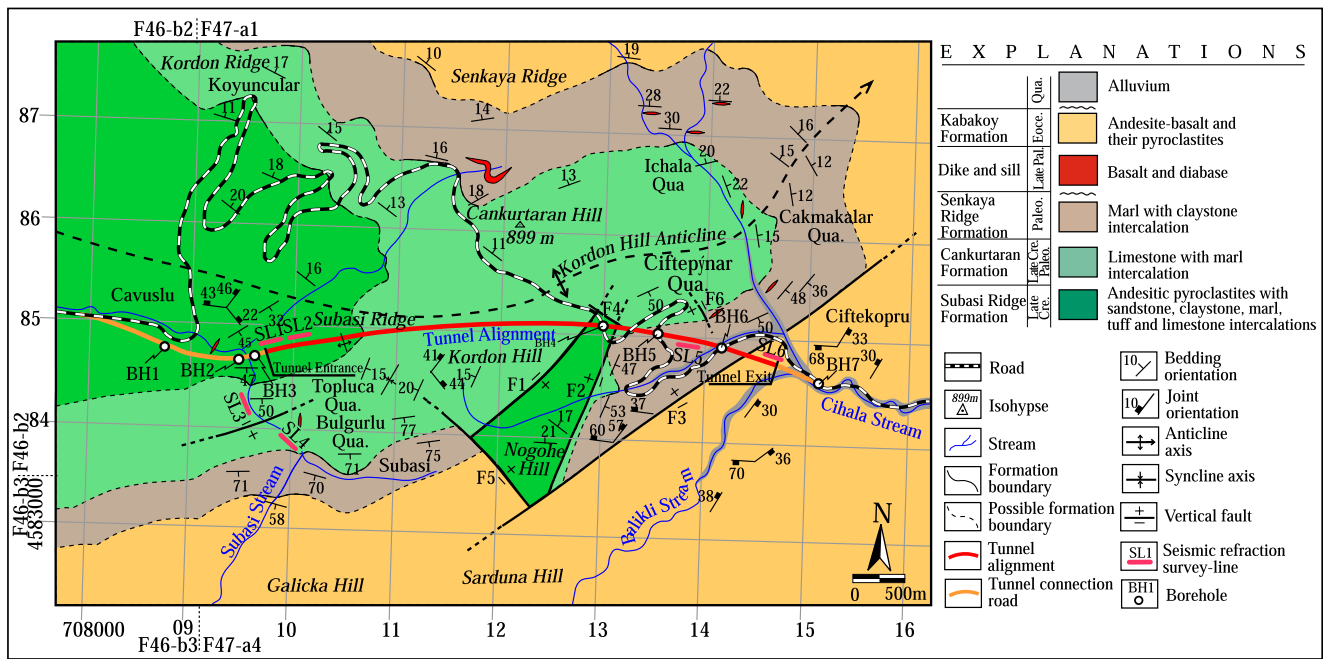


Fig. 3 Simplified geological map of close vicinity of the study area (modified from Capkinoglu 1981)

Discontinuity readings were taken from outcrops to identify the main discontinuity sets. The discontinuity orientations were identified by using the Dips v7.0 (Rocscience Inc. 2016a) software according to stereographic projection (Fig. 5 and Table 2). Additionally, the identification of the discontinuities in geotechnical units such as orientation, aperture, spacing, roughness, persistence, weathering degree and infilling were obtained by examining the core samples and scan-line surveys by the help of the technique recommended

by ISRM (2007). The quantitative descriptions of the discontinuities are shown in Table 3.

In the present study, the most commonly preferred classifications such as the RMR and Q system were employed to describe the ground throughout the tunnel route and to determine empirical lining design. The data acquired from field works, scan-line surveys, boreholes and laboratory studies were utilized in the classification systems.

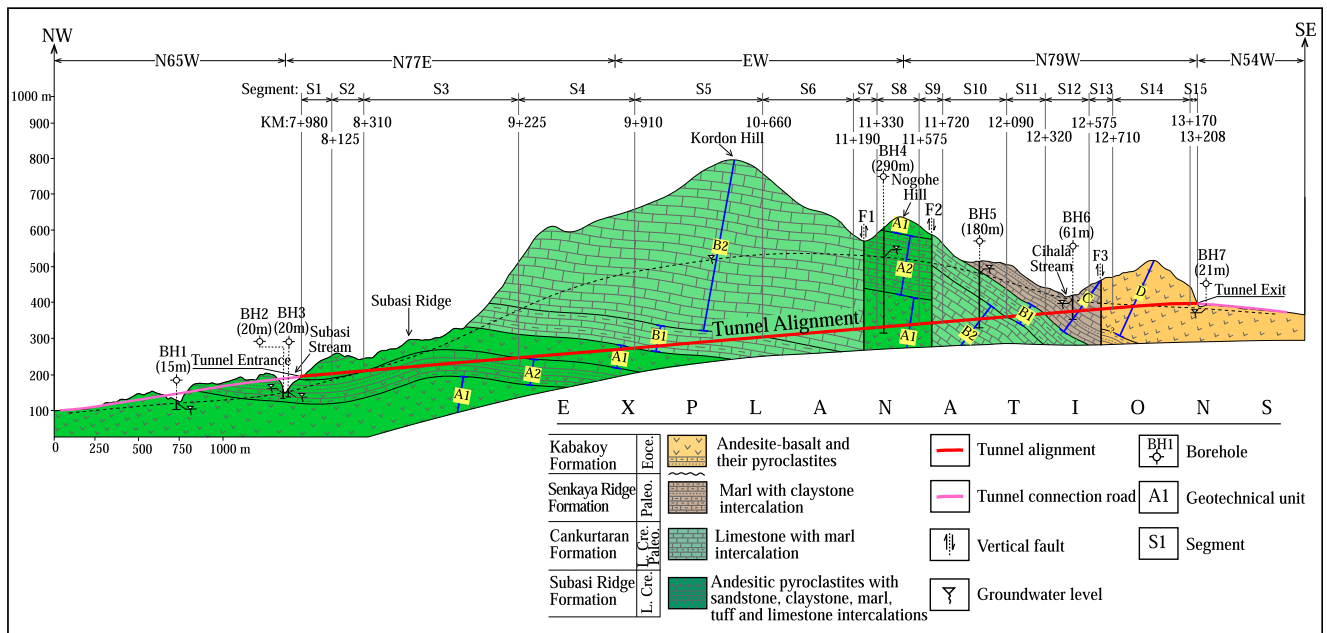


Fig. 4 Geological cross section showing the borehole locations, segments, chainages and geotechnical units along the tunnel alignment

Table 1 Physico-mechanical and elastic properties of rock materials, rock quality designation (RQD) and Lugeon values

Properties	Subasi Ridge Formation		Cankurtaran Formation		Senkaya Ridge Formation	Kabakoy Formation
	Unit A1	Unit A2	Unit B1	Unit B2	Unit C	Unit D
Unit weight (γ , kN/m ³)	(24.67–26.73) ^a 25.78	(20.80–24.67) ^a 22.97	(23.55–25.89) ^a 24.62		(18.95–24.73) ^a 22.73	(23.16–26.04) ^a 24.73
Uniaxial compressive strength (σ_{ci} , MPa)	(3.10–59.92) ^a 30.73	(27.59–253.95) ^a 109.71	(12.46–94.64) ^a 55.05		(5.37–56.31) ^a 26.19	(25.83–238.26) ^a 60.98
Point load strength index ($I_{S(50)}$, MPa)	(0.15–4.28) ^a 1.54	(1.38–12.70) ^a 5.49	(0.62–4.73) ^a 2.75		(0.27–2.82) ^a 1.31	(1.29–11.91) ^a 3.05
Young's modulus (E_r , GPa)	(13.27–29.50) ^a 18.45	(11.50–48.72) ^a 34.24	(15.00–34.75) ^a 27.25		(8.53–18.05) ^a 12.20	(17.23–55.08) ^a 27.53
Rock quality designation (RQD, %)	(59–98) ^a 84	(34–90) ^a 60	(36–94) ^a 62	(74–96) ^a 88	(0–8) ^a 3*	(25–96) ^a 73
Lugeon (Lu, l/min/m)	(0.92–5.74) ^a 2.86	(0.38–6.72) ^a 3.75	(0.00–1.08) ^a 0.32	(0.32–4.17) ^a 2.05	(0.00–0.32) ^a 0.12	(1.02–5.00) ^a 3.29

^a Average value

*The RQD value was selected as 10% in rock mass calculations according to Barton et al. (1974)

The RMR classification system was suggested by Bieniawski (1974) and updated by Bieniawski (1989). This classification system utilizes the following five rock mass parameters: strength of rock material, RQD, spacing of discontinuities, condition of discontinuities and groundwater. In order to determine the ratings for each five parameters, the charts for the RQD, intact rock strength and discontinuity spacing and rating tables suggested by Bieniawski (1989) were used. The basic RMR values were determined by the addition of these ratings. In the next stage, adjustments for the discontinuity orientations considering the tunnel excavation direction were applied to the basic RMR ratings. Based on the both basic and adjusted RMR values, the character of ground throughout the Cankurtaran Tunnel route varies between “very poor” and “fair” (Table 4).

The Q classification system was proposed by Barton et al. (1974) and it is determined by the following Eq. (1).

$$Q = \left(\frac{RQD}{J_n} \right) \left(\frac{J_r}{J_a} \right) \left(\frac{J_w}{SRF} \right) \quad (1)$$

where J_n is joint set number, J_r is joint roughness number, J_a is joint alteration number, J_w is joint-water reduction factor and SRF is stress reduction factor.

In terms of Q values, the characteristics of the rocks located throughout the tunnel alignment vary from “extremely poor” to “very poor” (Table 4).

To be on the safe side, the rock mass quality values of the fault zones F1-F2 and fault zone F3 were assumed as half of the rock mass quality values of the unit B2 and unit C, respectively. According to rock mass classifications, the results obtained from the Q system exhibited more conservative estimates than basic and adjusted RMR values owing to different input parameters. The main difference between the results of

these systems was originated from the lack of a stress parameter in the RMR system.

The rock mass parameters are essential data for the numerical modeling. To define the rock mass constants (m_b , s , a), the Hoek–Brown failure criterion was utilized. The RMR rating can be used to predict the Geological Strength Index (GSI) for RMR > 23. In this case, the modified Q value (Q') should be used. Therefore, the GSI values of the geotechnical units and fault zones were obtained using Eqs. (2) and (3) suggested by Hoek et al. (1995).

$$GSI = 9 \ln Q' + 44 \quad (2)$$

$$Q' = \left(\frac{RQD}{J_n} \right) \left(\frac{J_r}{J_a} \right) \quad (3)$$

Variation of the RQD, RMR, Q and GSI values along the tunnel route are depicted in Fig. 6.

Hoek–Brown constants were determined using Eqs. (4)–(6) proposed by Hoek et al. (2002).

$$m_b = m_i e^{\left(\frac{GSI-100}{28-14D} \right)} \quad (4)$$

$$s = e^{\left(\frac{GSI-100}{9-3D} \right)} \quad (5)$$

$$a = \frac{1}{2} + \frac{1}{6} \left(e^{-GSI/15} - e^{-20/3} \right) \quad (6)$$

where m_i is constant of the rock material and D is disturbance factor.

Factor of disturbance (D) was taken into account to be 0.5 for poor quality blasting and zero for the mechanical excavation. The m_i values of the rock materials were identified using the RocData v5.0 (Rocscience Inc. 2016b) software and were taken as 13, 7, 8, 8, 7 and 25 for unit A1, unit A2, unit B1, unit B2, unit C and unit D,

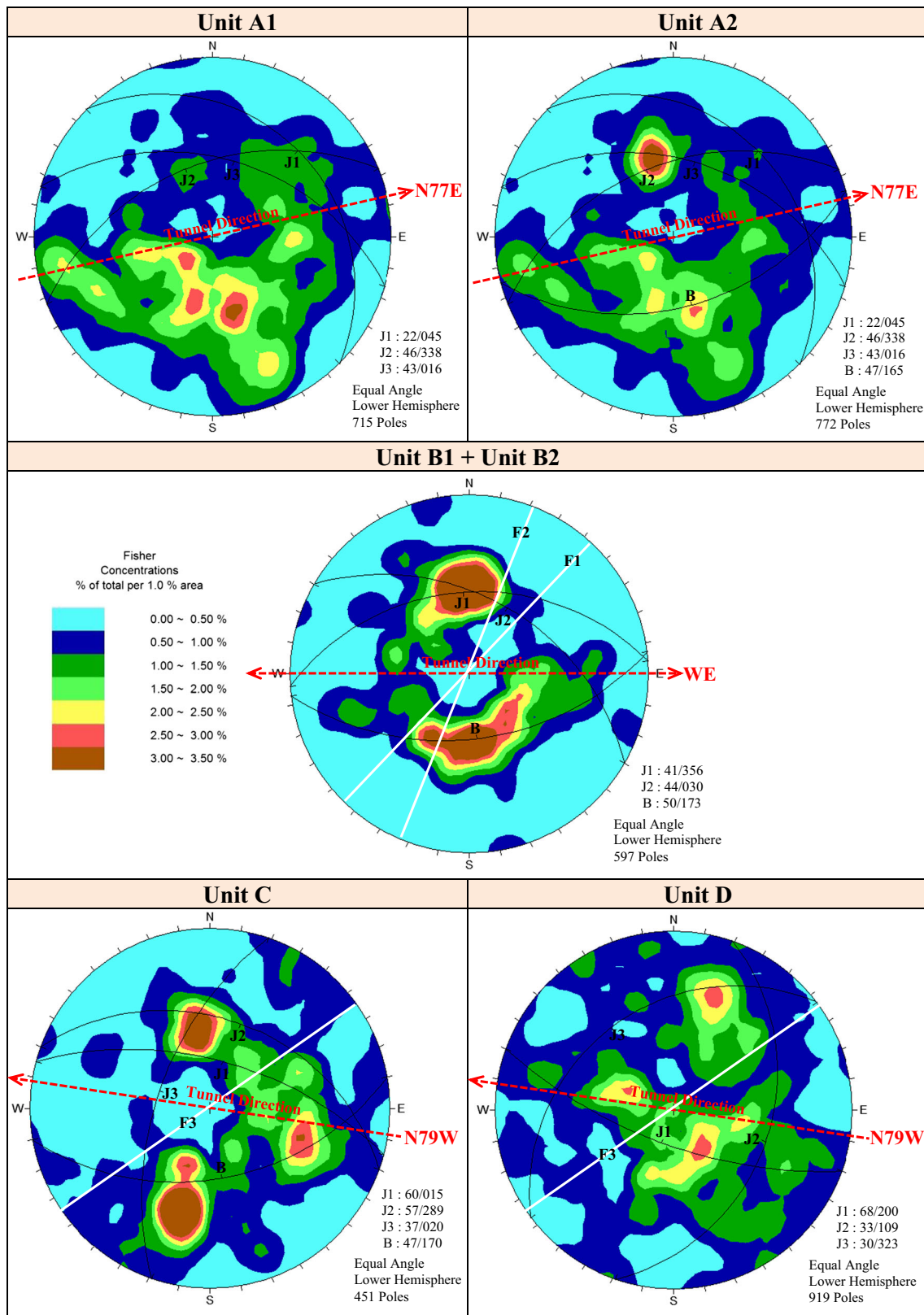


Fig. 5 Stereographic projection of the discontinuity sets in geotechnical units

Table 2 Orientations of the discontinuity sets

Formation	Geotechnical unit	Discontinuity type	Dip	Dip direction
Subasi Ridge Formation	Unit A1	Joint	22	045
		Joint	46	338
		Joint	43	016
	Unit A2	Joint	22	045
		Joint	46	338
		Joint	43	016
		Bedding	47	165
Cankurtaran Formation	Unit B1	Joint	41	356
	+	Joint	44	030
	unit B2	Bedding	50	173
Senkaya Ridge Formation	Unit C	Joint	60	015
		Joint	57	289
		Joint	37	020
		Bedding	47	170
Kabakoy Formation	Unit D	Joint	68	200
		Joint	33	109
		Joint	30	323

respectively (Table 5). It was assumed to be 7, 7 and 8 for intact rocks in fault zones F1, F2 and F3, respectively.

The rock mass strength (σ_{cm}) and deformation modulus (E_m) were obtained using Eqs. (7) and (8) proposed by Hoek et al. (2002) and Hoek and Diederichs (2006).

$$\sigma_{cm} = \sigma_{ci} \cdot \frac{(m_b + 4s - a(m_b - 8s))(m_b/4 + s)^{a-1}}{2(1+a)(2+a)} \text{ (MPa)} \quad (7)$$

$$E_m = E_i \left(\frac{1 - (D/2)}{1 + e^{(60+15D-GSI)/11}} \right) \text{ (GPa)} \quad (8)$$

where σ_{ci} is uniaxial compressive strength of intact rock in MPa and E_i is Young's modulus in GPa.

Because it is hard to determine the σ_{ci} and E_i values of intact rocks in fault zones due to sampling difficulties, the σ_{cm} and E_m values were estimated using Eqs. (9) and (10) that are the basis for the RMR proposed by Aydan et al. (1997). These equations are more suitable to identify the elastic properties of weak rocks such as phyllite, mudstone, siltstone, salt, potash or weathered and/or sheared/faulted rocks at relatively shallow depths (<400 m).

Table 3 Quantitative description of the discontinuities in geotechnical units

	Unit A1		Unit A2		Unit B1		Unit B2		Unit C		Unit D
	Joint	Bedding	Joint	Bedding	Joint	Bedding	Joint	Bedding	Joint	Joint	
Spacing (cm)	(0.5–240) ^a 13.31	(1–110) ^a 8.94	(0.5–240) ^a 13.31	(1–45) ^a 6.70	(1–84) ^a 13.53	(1–64) ^a 7.84	(1–84) ^a 27.06	(0.5–13) ^a 2.12	(0.5–33) ^a 4.28	(0.5–119) ^a 12.24	
Persistence (m)	(0.2–35) ^a 9.10	(4–50) ^a 24.45	(0.2–35) ^a 9.10	(12–40) ^a 21.20	(1–34) ^a 7.50	(12–40) ^a 21.20	(1–34) ^a 7.50	(4–50) ^a 27.11	(0.2–35) ^a 9.66	(1–22) ^a 5.18	
Aperture (mm)	(0–24) ^a 1.92	(0–6.5) ^a 0.99	(0–24) ^a 1.92	(5–35) ^a 12.39	(0–5) ^a 0.89	(0–1) ^a 0.19	(0–5) ^a 0.89	(0–5) ^a 1.05	(0–4) ^a 1.1	(0–22) ^a 2.67	
Infilling	<5 mm soft clay and calcite	<5 mm calcite	<5 mm soft clay and calcite	>5 mm soft clay and calcite	<5 mm soft clay and calcite	<5 mm soft clay and calcite	<5 mm soft clay and calcite	<5 mm soft clay	<5 mm soft clay	<5 mm soft clay	
Roughness	Rough, undulating	Smooth, undulating	Rough, undulating	Smooth, undulating	Rough, undulating	Smooth, undulating	Rough, undulating	Rough, planar	Rough, undulating	Rough, undulating	
Weathering	Slightly weathered	Fresh	Slightly weathered	Slightly weathered	Slightly weathered	Slightly weathered	Slightly weathered	Slightly weathered	Slightly weathered	Slightly weathered	
Groundwater condition	Dripping	Dripping	Dripping	Dripping	Dripping	Dripping	Dripping	Dripping	Dripping	Dripping	

^a Average

Table 4 RMR and Q classifications of the rock masses along the Cankurtaran Tunnel

Segment	Chainage (km)	Rock mass	Basic RMR	Adj. RMR	Q'	Q
1	7 + 980–8 + 125	Entrance portal (unit A1)	46.4	41.7/Fair	2.6	0.26/Very poor
2	8 + 125–8 + 310	Unit A1	46.4	41.7/Fair	5.3	0.70/Very poor
3	8 + 310–9 + 225	Unit A2	41.0	33.8/Poor	2.0	0.27/Very poor
4	9 + 225–9 + 910	Unit A1	46.4	41.7/Fair	5.3	0.70/Very poor
5	9 + 910–10 + 660	Unit B1	34.1	27.4/Poor	1.0	0.14/Very poor
6	10 + 660–11 + 255	Unit B2	45.2	37.8/Poor	3.7	0.49/Very poor
7	11 + 245–11 + 255	F1 fault zone	22.6	15.8/Very poor	1.8	0.24/Very poor
8	11 + 255–11 + 645	Unit A1	46.4	38.9/Poor	5.3	0.70/Very poor
9	11 + 645–11 + 655	F2 fault zone	22.6	15.8/Very poor	1.8	0.24/Very poor
10	11 + 655–12 + 090	Unit B2	45.2	37.8/Poor	3.7	0.49/Very poor
11	12 + 090–12 + 320	Unit B1	34.1	27.4/Poor	1.0	0.14/Very poor
12	12 + 320–12 + 645	Unit C	31.7	26.7/Poor	0.5	0.05/Extremely poor
13	12 + 645–12 + 655	F3 fault zone	15.9	11.1/Very poor	0.3	0.025/Extremely poor
14	12 + 655–13 + 170	Unit D	46.9	42.2/Fair	4.6	0.61/Very poor
15	13 + 170–13 + 208	Exit portal (unit D)	46.9	42.2/Fair	2.3	0.23/Very poor

RMR Rock mass rating

$$\sigma_{cm} = 0.0016RMR^{2.5} \text{ (MPa)} \tag{9}$$

$$E_m = 0.0097RMR^{3.54} / 1000 \text{ (GPa)}. \tag{10}$$

The post-peak attitude of a rock mass is an essential input in the numerical modeling of a tunnel, because it has an important influence on the excavation stability. Residual parameters of the rock mass are needed to design underground structures properly. Much investigation has been focused on the specification of peak parameters, and limited attempts have been made to predict the residual parameters of rocks. In this study, because no field testing was performed to investigate the post-peak behavior of geotechnical units upon excavation, it was estimated by the help of the method suggested by Cai et al. (2007). The residual GSI (GSI_r) value and residual Hoek–Brown constants (m_{br} , s_r , a_r) were calculated using Eqs. (11)–(14).

$$GSI_r = GSI e^{-0.0134GSI} \tag{11}$$

$$m_{br} = m_i e^{\left(\frac{GSI_r - 100}{28}\right)} \tag{12}$$

$$s_r = e^{\left(\frac{GSI_r - 100}{9}\right)} \tag{13}$$

$$a_r = \frac{1}{2} + \frac{1}{6} \left(e^{-GSI_r/15} - e^{-20/3} \right) \tag{14}$$

In order to determine the Poisson’s ratio (ν_m) of geotechnical units dynamically, geophysical studies were carried out using the seismic refraction method in six lines (Fig. 2). With the help of the seismic studies, primary-wave (V_p) and shear-wave (V_s) velocities were defined for each geotechnical unit cropped out along the tunnel alignment. Considering the elastic theory, the dynamic Poisson’s ratio was determined using the seismic velocity values (Eq. 15).

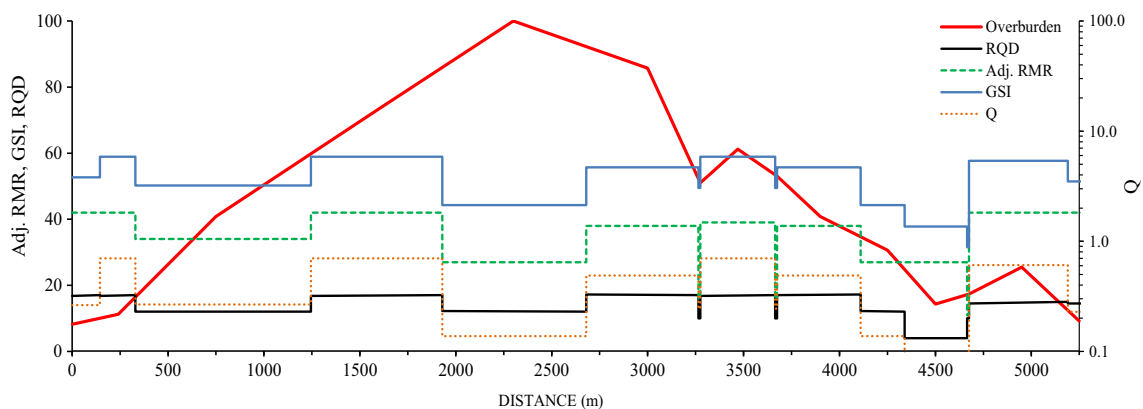


Fig. 6 Rock mass characterization along the Cankurtaran Tunnel

Table 5 Calculated rock mass parameters of the geotechnical units and fault zones for numerical analyses

	Entrance portal (unit A1)	Unit A1	Unit A2	Unit A1	Unit B1	Unit B2	F1 fault zone	Unit A1	F2 fault zone	Unit B2	Unit B1	Unit C	F3 fault zone	Unit D	Exit portal (unit D)
Segment	1	2	3	4	5	6	7	8	9	10	11	12	13	14	15
Elastic type	Isotropic	Isotropic	Isotropic	Isotropic	Isotropic	Isotropic	Isotropic	Isotropic	Isotropic	Isotropic	Isotropic	Isotropic	Isotropic	Isotropic	Isotropic
Rock mass strength, σ_{cm} (MPa)	4.80	5.70	14.11	5.70	5.37	7.43	3.89	5.70	3.89	7.43	5.37	1.97	1.60	14.93	12.68
Deformation modulus, E_m (GPa)	2.89	4.39	4.49	4.39	2.27	5.26	0.60	4.39	0.60	5.26	2.27	0.60	0.17	6.05	3.94
Poisson's ratio, ν_m	0.23	0.23	0.4	0.23	0.46	0.26	0.34	0.23	0.38	0.26	0.46	0.31	0.42	0.39	0.39
Material type	Plastic	Plastic	Plastic	Plastic	Plastic	Plastic	Plastic	Plastic	Plastic	Plastic	Plastic	Plastic	Plastic	Plastic	Plastic
m_i constant	13	13	7	13	8	8	8	13	8	8	8	7	7	25	25
GSI	53	59	50	59	44	56	49	59	49	56	44	38	32	58	51
m_b constant	1.37	1.84	0.94	1.84	0.56	0.97	1.32	1.84	1.32	0.97	0.56	0.36	0.61	3.33	2.47
s constant	0.0018	0.0042	0.0013	0.0042	0.0006	0.0027	0.00364	0.0042	0.0036	0.0027	0.0006	0.0002	0.000496	0.0035	0.0015
a constant	0.505	0.503	0.506	0.503	0.508	0.504	0.506	0.503	0.506	0.504	0.508	0.513	0.520	0.503	0.505
GSI _r	26	27	26	27	24	26	25	27	25	26	24	23	21	27	26
m_b residual constant	0.93	0.95	0.70	0.95	0.54	0.58	0.56	0.95	0.56	0.58	0.54	0.44	0.41	1.82	1.77
s_r residual constant	0.00027	0.00029	0.00026	0.00029	0.00023	0.00028	0.00025	0.00029	0.00025	0.00028	0.00023	0.00019	0.000148	0.00029	0.00026
a_r residual constant	0.529	0.528	0.530	0.528	0.532	0.528	0.530	0.528	0.530	0.528	0.532	0.536	0.542	0.528	0.530
Disturbance factor (D)	0.5	0.5	0.5	0.5	0.5	0.5	0	0.5	0	0.5	0.5	0.5	0	0.5	0.5
Dilation parameter	0	0	0	0	0	0	0	0	0	0	0	0	0	0	0
Overburden (m)	40	55	200	360	490	420	250	300	260	200	150	70	85	125	45
Vertical stress, σ_v (MPa)	1.03	1.42	4.59	9.28	12.06	10.34	5.00*	7.73	5.20*	4.92	3.69	1.59	1.70*	3.09	1.11
Horizontal stress, σ_h (MPa)	0.31	0.42	3.06	2.77	10.28	3.64	5.00	2.31	5.20	1.73	3.15	0.72	1.70	1.98	0.71

*Unit weight was selected arbitrarily as 20 kN/m³ for fault zone material

GSI Geological Strength Index

$$\nu_m = \frac{V_p^2 - 2V_s^2}{2(V_p^2 - V_s^2)} \tag{15}$$

where V_p is primary-wave velocity in m/s and V_s is shear-wave velocity in m/s.

Because the seismic studies were not feasible in the fault zones due to the steep morphology, the Poisson’s ratio values of the fault zones were estimated using the empirical equation (Eq. 16) that is the basis for the rock mass strength suggested by Aydan et al. (1993). The given equation gives the best solution for weak, weathered and/or faulted rocks at shallow depths (<400 m).

$$\nu_m = 0.25 \left(1 + e^{-\sigma_{cm}/4} \right) \tag{16}$$

where σ_{cm} is rock mass strength in MPa.

The rock mass parameters of the geotechnical units and fault zones are presented in Table 5. These parameters were later used in the FEM analyses as input parameters.

The vertical stress (σ_v) acting at a point below the ground surface is due to the weight of overburden. The loading condition for vertical stress was calculated by:

$$\sigma_v = \gamma H \text{ (MPa)} \tag{17}$$

where γ is rock mass unit weight in MN/m³ and H is overburden depth in meters.

The horizontal stresses (σ_h) acting on a rock element at a depth below the surface are harder to predict than the vertical stresses. The horizontal stress in fractured rock mass was obtained from the following Eq. (18) proposed by Sheorey et al. (2001). On the other hand, the horizontal stress in the fault zones was assumed to be equal to the vertical stress. The rock mass parameters considered in the analysis models are given in Table 5.

$$\sigma_h = \frac{\nu_m}{1-\nu_m} \sigma_v + \frac{\beta E_m G}{1-\nu_m} (H + 1000) \text{ (MPa)} \tag{18}$$

where $\beta = 8 \times 10^{-6} \text{ }^\circ\text{C}$ (coefficient of linear thermal expansion), $G = 0.024 \text{ }^\circ\text{C/m}$ (geothermal gradient), ν_m is the Poisson’s ratio of rock mass and E_m is deformation modulus of rock mass in GPa.

Tunnel lining design

Bieniawski (1989) published a set of guidelines for the selection of support in tunnels in rock for which the RMR value has been defined. The support chart is applied only for a tunnel with a 10-m horseshoe-shaped span, excavated using drill-blast technique and in situ stress <25 MPa. However, in the Q system, there are no specific limitations such as span of underground openings and excavation shape. Therefore, because of restrictions of the RMR system, the empirical support

systems (final lining) recommended by Q classification (Barton, 2002) were implemented for the Cankurtaran Tunnel. Based on the Q system values, four support categories were determined for 15 segments (Table 6). The planned construction properties, including round length, construction phase, support time and stand-up time, determined considering the adjusted RMR ratings are also given in Table 6.

To clutch the process of tunnel lining design, it is important to investigate basic notions of how a rock mass around an opening deforms and how the supports check this deformation. Therefore, the convergence–confinement (CC) method was utilized to determine the interaction among the surrounding rock mass and lining support. This methodology, which satisfies the Hoek–Brown criterion, has been delineated by Carranza-Torres and Fairhurst (1999) for rock masses. The CC method authorizes the load charged on a lining applied behind the tunnel face to be predicted. In this method, uniform internal pressure p_i and far-field stress σ_o are taken into account. The P_i and S_o are described as (Carranza-Torres and Fairhurst 2000);

$$P_i = \frac{p_i}{m_b \sigma_{ci}} + \frac{s}{m_b^2} \text{ (MPa)} \tag{19}$$

$$S_o = \frac{\sigma_o}{m_b \sigma_{ci}} + \frac{s}{m_b^2} \text{ (MPa)} \tag{20}$$

where m_b and s are the Hoek–Brown constants, σ_{ci} is the intact rock strength in MPa, p_i is the support pressure (uniform internal) in MPa, σ_o is the far-field stress ($\sigma_o = (\sigma_v + \sigma_h)/2$) in MPa, P_i is scaled internal pressure in MPa and S_o is scaled far-field stress in MPa.

The scaled critical internal pressure P_i^{cr} representing the elastic limit and the actual critical internal pressure p_i^{cr} are defined as (Carranza-Torres and Fairhurst 2000);

$$P_i^{cr} = \frac{1}{16} \left[1 - \sqrt{1 + 16S_o} \right]^2 \text{ (MPa)} \tag{21}$$

$$p_i^{cr} = \left[P_i^{cr} - \frac{s}{m_b^2} \right] m_b \sigma_{ci} \text{ (MPa)} \tag{22}$$

If the p_i is less than the p_i^{cr} , failure is expected to occur. On the other hand, if the p_i is greater than this p_i^{cr} , no failure will occur.

In this study, the CC analyses were carried out in two stages. In the first stage, the p_i was supposed to be 0 for the unsupported state. The essential rock characteristics were replaced due to the rock units and they were utilized as data. The computed values of each segment are presented in Table 7. When p_i and p_i^{cr} values are compared for unsupported tunnel segments, apart from segments 2 and 15, the stability problem is expected, and the deformation type is plastic.

In the second stage, the p_s^{max} (maximum pressure) and the K_s (elastic stiffness) of the proposed lining supports were defined for each segment. In calculations, the methods suggested

Table 6 Empirical tunnel support categories (final lining) for the rock masses along the Cankurtaran Tunnel

Support type	0.4 < Q < 1 /Poor rock	0.1 < Q < 0.4 /Poor rock	0.04 < Q < 0.1 /Extremely poor	0.01 < Q < 0.04 /Extremely poor
Segment	2, 4, 6, 8, 10, 14	1, 3, 5, 7, 9, 11, 15	12	13
Construction phase	Top heading and bench	Top heading and bench	Top heading, bench and invert	Top heading, bench and invert
Excavation method	Drill and blast	Drill and blast	Mechanical excavation	Mechanical excavation
Round length	1.5–3.0-m advance in top heading and bench	1.0–1.5-m advance in top heading and bench	0.5–1.0-m advance in top heading, bench and invert	0.5–1.0-m advance in top heading, bench and invert
Stand-up time	Immediate collapse	Immediate collapse	Immediate collapse	Immediate collapse
Support time	Install support concurrently with excavation	Install support concurrently with excavation	Install support concurrently with excavation	Install support concurrently with excavation
Support requirements				
Roof	Systematic rock bolts 4 m long, spaced 1.5–1.7 m and 90–120-mm-thick steel fiber/wire mesh-reinforced shotcrete (Sfr + B)	Systematic rock bolts 4 m long, spaced 1.3–1.5 m and 120–150-mm-thick steel fiber/wire mesh-reinforced shotcrete (Sfr + B)	Systematic rock bolts 4 m long, spaced 1.2–1.3 m and 150–250-mm-thick steel fiber/wire mesh-reinforced shotcrete (Sfr + B) and steel ribs (RRS)	Systematic rock bolts 4 m long, spaced 1.0–1.2 m and 150–250-mm-thick steel fiber/wire mesh-reinforced shotcrete (Sfr + B) and steel ribs (RRS)
Wall	Systematic rock bolts 3.5 m long, spaced 1.7–2.1 m and 50–90-mm-thick steel fiber/wire mesh-reinforced shotcrete (Sfr + B)	Systematic rock bolts 3.5 m long, spaced 1.5–1.7 m and 90–120-mm-thick steel fiber/wire mesh-reinforced shotcrete (Sfr + B)	Systematic rock bolts 3.5 m long, spaced 1.2–1.3 m and 150–250-mm-thick steel fiber/wire mesh-reinforced shotcrete (Sfr + B) and steel ribs (RRS)	Systematic rock bolts 3.5 m long, spaced 1.0–1.2 m and 150–250-mm-thick steel fiber/wire mesh-reinforced shotcrete (Sfr + B) and steel ribs (RRS)
Invert	–	–	150–250-mm-thick steel fiber/wire mesh-reinforced shotcrete (Sfr + B) and steel ribs (RRS)	150–250-mm-thick steel fiber/wire mesh-reinforced shotcrete (Sfr + B) and steel ribs (RRS)

by Hoek (2007) and Carranza-Torres and Engen (2017) were used. According to the acquired results, the p_s^{max} values were higher than the p_i^{cr} values for segments 1, 2, 3, 10, 12, 14, and 15. However, the p_s^{max} values were smaller than the p_i^{cr} values for other segments. As a result, considering the CC analysis, the empirical lining design was not satisfactory for these segments.

Numerical analyses have been progressively used today compared to the past in tunnel designs to check the accuracy of results acquired from empirical methods owing to the quick developments in computer systems. Because numerical techniques consider the geometry of tunnels, field stresses and elastic/strength parameters, they are valuable design instruments in tunneling. The finite element method (FEM) has become one of the most chosen methods in underground applications by many researchers (i.e. Ozsan and Karpuz 2001; Javadi and Snee 2002; Kockar and Akgun 2003; Ozsan and Basarir 2003; Park 2004; Sari and Pasamehmetoglu 2004; Basarir et al. 2005; Basarir 2006; Genis et al. 2007; Gurocak et al. 2007; Sopaci and Akgun 2008; Kaya et al. 2011; Aydin et al. 2014; Kanik et al. 2015; Yalcin et al. 2015; Kaya and Sayin 2017; Lin et al. 2017; Ozdogan et al. 2018; Kanik and Gurocak 2018).

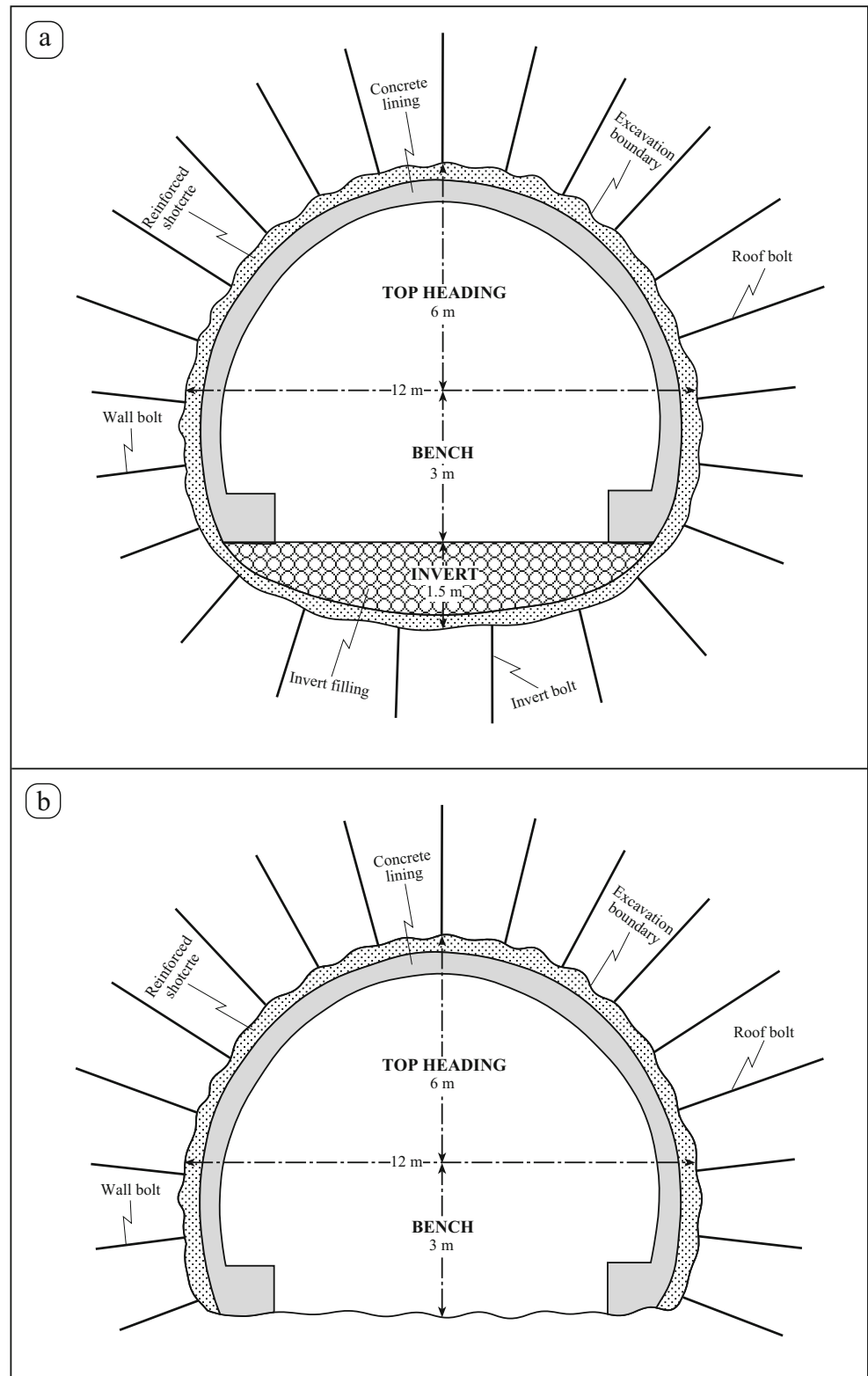
In the present study, to define the displacements and plastic zones around the opening and to check the validity of the suggested tunnel lining design given in Table 6, the 2D

FEM software RS² v9.0 and 3D FEM software RS³ v1.0 (Rocscience Inc. 2016c, 2017) were used in the numerical analyses. Unlike the RS³, RS² uses a plane strain analysis where two principal in situ stresses are in the plane of the excavation, and the third principal stress is out of plane. In this model, the 3D stress tensor is divided into three orthogonal stresses which are aligned with the 2D model of excavation (2 in plane and 1 out of plane), and they decompose. An automatic mesh around the excavation was formed, and considering the elasto-plastic analysis, deformations and stresses were calculated using these software programs. A very simple model was used to analyze the tunnel stability and to identify the concept of rock support interaction. The six-noded triangular elements were applied to optimize the meshes, and sensitive zoning was used around the excavation. The boundary of excavation was generated based on its height and span in three steps as (i) top heading, (ii) bench and (iii) invert for the “unit C” and fault zone F3 (segments 12 and 13), and (i) top heading and (ii) bench for the other segments (Fig. 7). The external boundary of design was applied as ten times the excavation width. The Hoek–Brown failure criterion was applied to define the yielded elements and plastic zones in close vicinity to the excavation. In general, deformation of the rock mass reaches its maximum rate between one and two circular tunnel radii behind the face (Hoek 2007). However, noncircular tunnel cross sections are widespread in application.

Table 7 Results of the convergence–confinement analyses for the Cankurtaran Tunnel

Segment	Entrance portal (unit A1)		Unit A1		Unit B1		Unit B2		F1 fault zone		Unit A1		Unit B2		F2 fault zone		Unit B1		Unit C		F3 fault zone		Unit D		Exit portal (unit D)	
	1	2	3	4	5	6	7	8	9	10	11	12	13	14	15	16	17	18	19	20	21	22	23	24	25	26
Uniform internal pressure, p_i (MPa)	0	0	0	0	0	0	0	0	0	0	0	0	0	0	0	0	0	0	0	0	0	0	0	0	0	0
Far-field stress, σ_o (MPa)	0.67	0.92	3.83	6.03	11.17	6.99	5.00	5.02	5.20	3.33	3.42	1.15	1.70	2.53	0.91											
Scaled far-field stress, S_o (MPa)	0.02	0.02	0.04	0.11	0.36	0.13	0.14	0.09	0.15	0.07	0.11	0.12	0.22	0.01	0.01											
Equivalent diameter, D (m)	10.76	10.76	10.76	10.76	10.76	10.76	10.76	10.76	10.76	10.76	10.76	10.76	11.22	11.22	10.76											
Equivalent radius, R (m)	5.38	5.38	5.38	5.38	5.38	5.38	5.38	5.38	5.38	5.38	5.38	5.38	5.61	5.61	5.38											
Scaled critical internal pressure, P_i^{cr} (MPa)	0.00101	0.00108	0.00467	0.02651	0.16113	0.03725	0.04008	0.01979	0.04256	0.01153	0.02816	0.03296	0.07678	0.00060	0.00015											
Actual critical internal pressure, p_i^{cr} (MPa)	0.002	0.0	0.325	1.428	4.942	1.835	1.375	1.048	1.465	0.461	0.816	0.294	0.599	0.056	0.0											
Maximum support pressure provided by shotcrete, P_{sc}^{max} (MPa)	0.55	0.44	0.55	0.44	0.55	0.44	0.55	0.44	0.55	0.44	0.55	0.44	0.87	0.44	0.55											
Elastic stiffness of shotcrete, K_{sc} (MPa/m)	0.11	0.09	0.11	0.09	0.11	0.09	0.11	0.09	0.11	0.09	0.11	0.17	0.17	0.09	0.11											
Maximum support pressure provided by rock bolt, P_{sb}^{max} (MPa)	0.148	0.111	0.148	0.111	0.148	0.111	0.148	0.111	0.148	0.111	0.148	0.250	0.250	0.111	0.148											
Elastic stiffness of rock bolt, K_{sb}^{max} (MPa/m)	0.02	0.01	0.02	0.01	0.02	0.01	0.02	0.01	0.02	0.01	0.02	0.03	0.03	0.01	0.02											
Maximum support pressure provided by steel set, P_{ss}^{max} (MPa)	–	–	–	–	–	–	–	–	–	–	–	–	–	–	–											
Elastic stiffness of steel set, K_{ss} (MPa/m)	–	–	–	–	–	–	–	–	–	–	–	–	–	–	–											
Maximum support pressure provided by combined support, P_s^{max} (MPa)	0.13	0.10	0.13	0.10	0.13	0.10	0.13	0.10	0.13	0.10	0.13	0.250	0.250	0.10	0.13											
Elastic stiffness of combined support, K_s (MPa/m)	4.93	4.93	4.93	4.93	4.93	4.93	4.93	4.93	4.93	4.93	4.93	4.93	4.93	4.93	4.93											
Maximum elastic deformation of the combined support, u_t^{max} (m)	0.64	0.51	0.64	0.51	0.64	0.51	0.64	0.51	0.64	0.51	0.64	0.01	0.01	0.51	0.64											

Fig. 7 Tunnel excavation sections for segments (a) 1–11 and 14–15, and (b) 12–13



Therefore, based on the method proposed by Curran et al. (2003) for noncircular cross sections, the slice thickness was taken as 10 m in the 3D models.

All rock masses contain joints. Representation of these joints in numerical models differs based on the model type

(discontinuum or continuum models). The fundamental significance in discontinuum models is the acting of discontinuity behavior. However, joints in continuum models are shown implicitly, with the intention that the behavior of the continuum design is substantially equivalent to the real jointed rock

mass being represented. Continuum models assume material is continuous throughout the body. Joints are treated as special cases by introducing interfaces among continuum bodies (Wyllie and Mah 2004). Because the discontinuity spacing values of the geotechnical units varied between close and very close (Table 3), the rock masses surrounding the excavation are well-suited for use in the continuum model. Therefore, in numerical analyses, continuum models were used to represent rock mass behavior in the 15 segments. In this study, numerical modeling consisted of three stages.

In the first and second stages, deformations (Figs. 9, 10, 11, 12 and 13) and plastic zones (Figs. 14, 15, 16, 17 and 18) that occurred around the openings were examined using top heading followed by excavating the entire tunnel (bench/invert). In the final stage, the effectiveness of the lining support (i.e., shotcrete, rock bolting and steel set) was analyzed.

According to the 2D models for unsupported cases, the maximum value of total displacement for all segments ranges between 0.23 and 17.71 cm (Table 8, Fig. 8). On the other hand, the maximum total displacements are very small, and range between 0.19 and 3.42 cm when considering the 3D analyses (Table 8, Fig. 8). It was seen that higher deformations occurred in the 2D models of segments 5, 8 and 12 compared to the 3D models (Fig. 8). Moreover, there is a discrepancy among the convergence system of the 2D and 3D analysis results for segment 4. An exaggerated displacement has developed at the external walls considering the 2D model of segment 4. However, no wall deformations were detected in the 3D models of segment 4 (Fig. 10). This is a quirky finding and an unforeseen outcome of the 2D model since small deformations at the tunnel walls possibly occur under low field stresses. In general, the deformation concentrations in the 2D designs are larger than those of the 3D design. The justification in these variations may be that in the 2D design, the tunnel opening upright to the plane is infinitive. In addition to this, in the analogous direction, the excavation round is merely 10 m in the 3D designs. Figure 8 shows the maximum total displacement (U_t), normalized vertical displacement (U_v/span) and normalized horizontal displacement ($U_h/\text{tunnel height}$) as a function of vertical distance. Each of the 15 plots corresponds to a different value of displacement. The plots clearly showed that an increase in field stress leads to higher displacement in segments 5, 8 and 12.

Strain is described as the ratio of tunnel closure to span. Hoek and Marinos (2000) proposed that for rock masses with strains less than 1%, few matters in terms of stability can possibly occur. On the other hand, minor squeezing problems are expected with strain values between 1 and 2.5%. In the present study, according to the 2D models, the strain values of 15 segments ranged between 0.05 and 2.22% (Table 8). However, the strain values obtained from 3D models varied between 0.03 and 0.57%, as shown in Table 8. According to 2D models, minor squeezing problems are expected in

segments 5, 6 and 8 due to the great field stresses. However, considering the 3D models, few stability problems are expected in all segments. Thus, the lining application (rock bolts and shotcrete; sometimes steel ribs) is recommended for the security of rock masses whose quality ranges between extremely poor and very poor along the Cankurtaran Tunnel route.

On the other hand, it should be remembered that RS² and RS³ are small-strain software programs and, thus, they cannot provide the very large strains. Therefore, it is more appropriate to take into account the size of the failure area rather than the deformation size. It can be seen from Figs. 14, 15, 16, 17 and 18 that the extent of the plastic zones demonstrates that there would be a serious matter in terms of stability, especially in segments 4–13, if they are not supported. When Figs. 15 and 16 and Table 8 are checked, the most problematical sections along the tunnel route are segments 4, 5, 6 and 8 driven in the units A1, B1, B2 and A1, respectively. A larger plastic zone and maximum total displacement were developed in these segments. However, the extents of plastic zones in the fault zones (F1, F2 and F3) are nearly half of these segments and are 6.29, 6.14 and 6.43 m, respectively (Table 8). In general, the maximum plastic zone concentrations occurred at the tunnel roof due to the raised field stresses. Considering the 2D designs, the dimensions of the plastic zone for segments varied between 1.22 and 14.21 m. On the other hand, since there is no a ruler option in RS³ v1.0, the failed areas in the 3D modeling could not be measured. In contrast, when the plastic zones occurred around the opening, given in Figs. 14, 15, 16, 17 and 18, are compared, it can be understood that the dimension of the failure areas in the 3D designs are partially larger than that of the 2D models, particularly in segments 5, 12, 13 and 15. This result is primarily owing to the lost arching activity in the 2D designs. It is believed that in numerical modelling, these distinctions are reasoned by a finite discretization.

In the last step, the efficiency of the suggested lining support was examined utilizing the same 2D and 3D analysis models. The lining designs were the same as those suggested in Table 6, and their properties implemented in FEM models are given in Table 9. Variances in the deformations and dimensions of the plastic zones following the support installations were analyzed, and outcomes were cross-checked with the unsupported states. The load split option in RS² v9.0 software authorizes the user to “split” the field stress-induced load, between any stages of the model, rather than applying the entire field stress load in the first stage. Therefore, the load splitting option is used to liken the retarded support installation. However, RS³ v1.0 software does not have a load split option. Therefore, in order to compare the 2D and 3D analyses results realistically, it was implicitly assumed that the lining is installed instantly after excavation, and that no deformation occurs before the support installation.

Table 8 Results of the 2D and 3D FEM analyses for the Cankurtaran Tunnel

Segments	Entrance portal (unit A1)		Unit A2		Unit A1		Unit B1		Unit B2		F1 fault zone		Unit A1		F2 fault zone		Unit B1		Unit C		F3 fault zone		Unit D		Exit portal (unit D)		
	1	2	3	4	5	6	7	8	9	10	11	12	13	14	15	16	17	18	19	20	21	22	23	24	25	26	27
2D-strain (ϵ , %)	0.05	0.06	0.21	0.97	2.95	2.17	0.24	1.72	0.26	0.53	0.38	0.76	0.16	0.76	0.08	0.04											
2D unsupported total displacement (U_t , cm)	0.31	0.38	1.28	5.80	17.71	12.99	1.46	10.30	1.54	3.19	2.28	4.55	0.94	4.55	0.50	0.23											
2D unsupported vertical displacement (U_x , cm)	0.30	0.37	1.25	4.66	14.58	12.84	1.46	9.69	1.54	3.17	2.27	4.40	0.84	4.40	0.61	0.22											
2D unsupported horizontal displacement (U_y , cm)	0.31	0.35	1.08	4.88	15.43	6.62	1.28	6.13	1.36	1.75	2.07	3.81	0.89	3.81	0.50	0.21											
2D-supported total displacement (U_t , cm)	0.30	0.36	1.08	4.10	13.30	8.81	1.28	8.55	1.37	3.11	1.94	1.00	0.32	1.00	0.50	0.22											
2D-supported vertical displacement (U_x , cm)	0.29	0.36	1.07	3.97	13.15	8.71	1.28	8.46	1.36	3.11	1.94	0.36	0.32	0.36	0.61	0.22											
2D supported horizontal displacement (U_y , cm)	0.28	0.26	0.76	3.12	11.95	4.01	0.57	3.43	0.64	1.08	1.36	0.99	0.23	0.99	0.50	0.19											
2D unsupported plastic zone (R_{pt} , m)	1.83	1.87	2.78	13.83	14.21	11.75	6.29	13.97	6.14	5.69	6.08	7.05	6.43	7.05	2.57	1.22											
2D supported plastic zone (R_{pt} , m)	1.17	0.81	0.58	4.90	6.61	4.79	3.09	3.21	3.41	2.70	1.97	0.00	1.39	0.00	0.58	0.49											
3D strain (ϵ , %)	0.04	0.05	0.11	0.57	0.53	0.49	0.10	0.44	0.10	0.21	0.20	0.26	0.05	0.26	0.06	0.03											
3D unsupported total displacement (U_t , cm)	0.24	0.30	0.68	3.42	3.20	2.94	0.57	2.61	0.59	1.25	1.17	1.55	0.30	1.55	0.36	0.19											
3D unsupported vertical displacement (U_x , cm)	0.17	0.20	0.53	2.38	2.73	2.16	0.42	1.89	0.42	0.80	0.92	1.39	0.27	1.39	0.28	0.15											
3D unsupported horizontal displacement (U_y , cm)	0.23	0.29	0.68	3.39	3.15	2.81	0.57	2.59	0.59	1.19	1.06	1.55	0.28	1.55	0.36	0.19											
3D supported total displacement (U_t , cm)	0.14	0.15	0.40	1.84	3.03	1.76	0.30	1.37	0.29	0.56	0.62	0.56	0.15	0.56	0.29	0.10											
3D supported vertical displacement (U_x , cm)	0.14	0.15	0.36	1.32	2.03	1.18	0.21	1.05	0.21	0.47	0.46	0.55	0.12	0.47	0.20	0.10											
3D supported horizontal displacement (U_y , cm)	0.11	0.13	0.40	1.84	3.01	1.76	0.30	1.37	0.29	0.56	0.62	0.28	0.15	0.56	0.29	0.10											

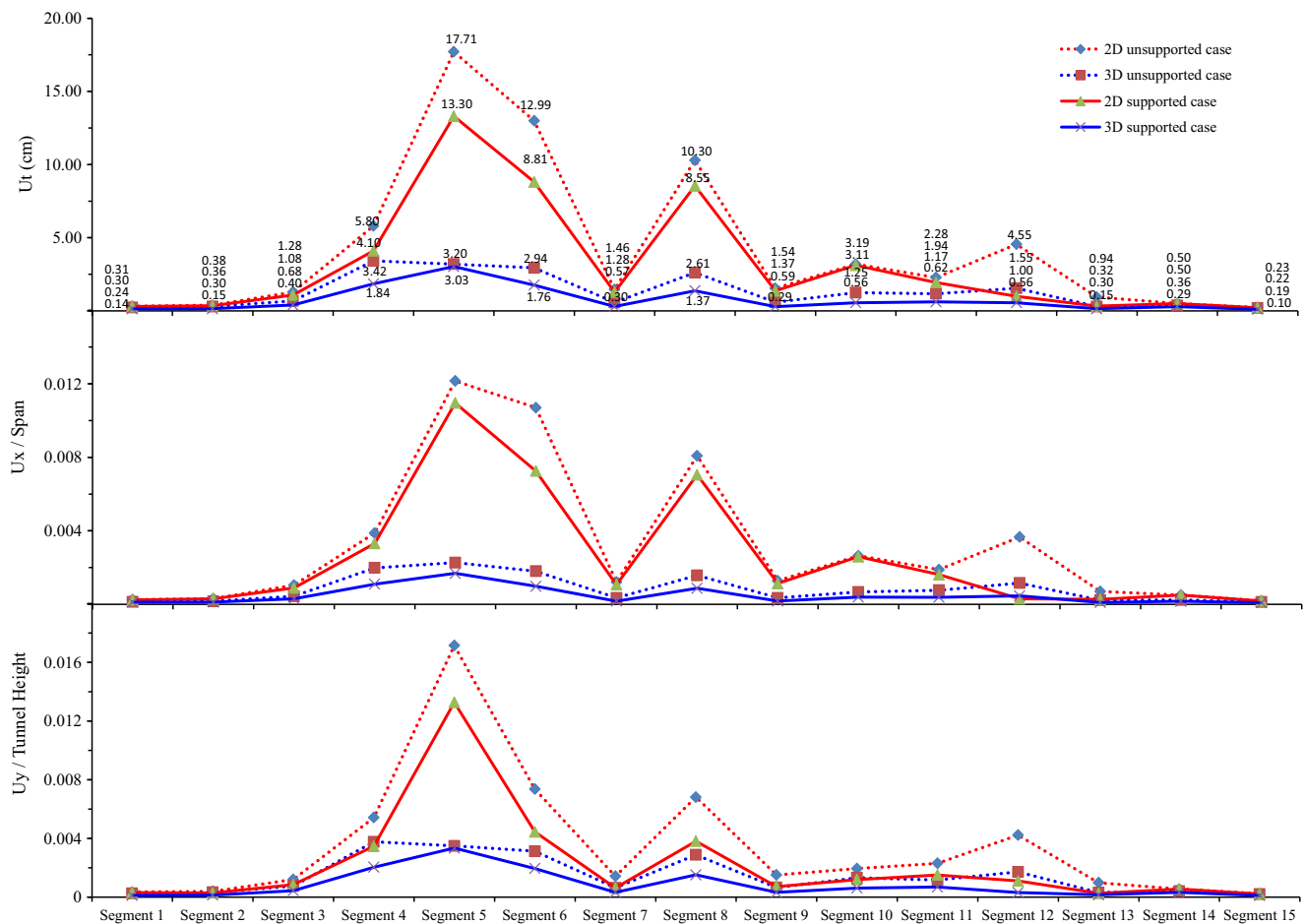


Fig. 8 Graphs showing the maximum total displacement (U_t), vertical displacement (U_x)/span and horizontal displacement (U_y)/tunnel height variations along the tunnel line for unsupported and supported cases according to 2D and 3D numerical analyses

The maximum total displacements for all supported segments range between 0.22 and 13.30 cm, and 0.10 and 1.84 cm with respect to 2D and 3D analyses, respectively. The size of the displacements was indistinctly decreased after support installation (Fig. 8, Table 8). It was concluded that no crown and wall displacements occurred in the 2D models of

segments 6–10 compared to the 3D models (Figs. 10, 11 and 12). However, in the 2D models of segments 1, 4, 12 and 15, an overdone deformation condensation demonstrating a failure formed at the external walls. In contrast to the 2D FEM models, the reasonable deformations in the 3D analysis results of all segments occurred inside the reinforced area, and these

Table 9 Characteristics of the support units used in the numerical analyses (TGDH 2013)

Properties	Shotcrete	Wire mesh	Rock bolt	Steel set
Young's modulus (E , GPa)	20	200	200	200
Poisson's ratio (ν)	0.2	0.35	–	0.35
Peak uniaxial compressive strength (σ_{cp} , MPa)	20	400	–	400
Residual uniaxial compressive strength (σ_{cr} , MPa)	3.5	–	–	–
Peak tensile strength (σ_{tp} , MPa)	3.1	500	–	500
Residual tensile strength (σ_{tr} , MPa)	0	–	–	–
Peak load (MN)	–	–	0.25	–
Residual load (MN)	–	–	0.025	–
Type	–	Ø6.5 mm, 150 × 150 mm	Ø28 mm fully bonded	I-beam 160 cm × 17.9 kg/m

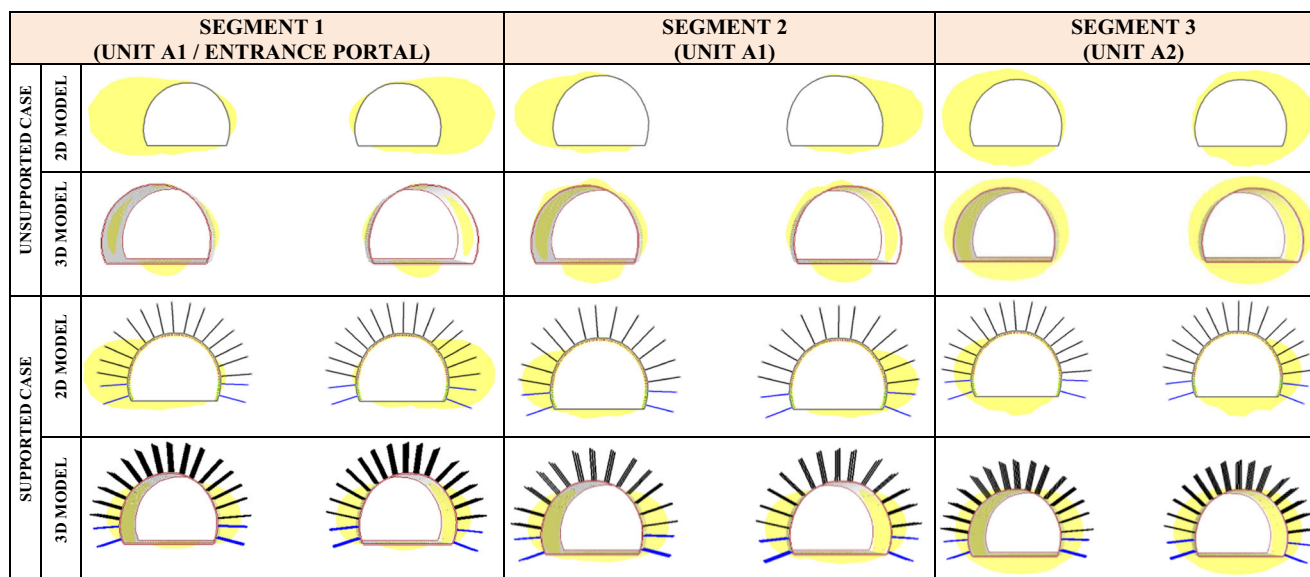


Fig. 9 2D and 3D numerical analyses showing the maximum total displacement developed in segments 1, 2 and 3 for the unsupported and supported cases

results verify the stability of the tunnel (Figs. 9, 10, 11, 12 and 13).

Furthermore, checking against an unsupported state, the size of the plastic zone has been decreased remarkably by implementation of the rock bolts and shotcrete for all tunnel segments (Figs. 14, 15, 16, 17 and 18). Following the application of lining, the size of the plastic zone determined in the 2D designs of all segments reduced from 1.22–14.21 m to 0.00–6.61 m. However, as it may be observed from the 3D

models shown in Figs. 14, 15, 16, 17 and 18, the plastic zones hardly ever formed. The empirical lining applications have been efficient in decreasing the plastic zone around the most problematic segments 7, 9 and 13 driven in fault zones (Figs. 16 and 18). The extremely poor rock mass quality of segments 12 and 13 was supported by the heaviest lining, including steel ribs. According to 3D analysis results of segments 4, 6 and 8, there are still plastic zones at the crown level, as in the 2D model (Figs. 15 and 16). Considering the 3D

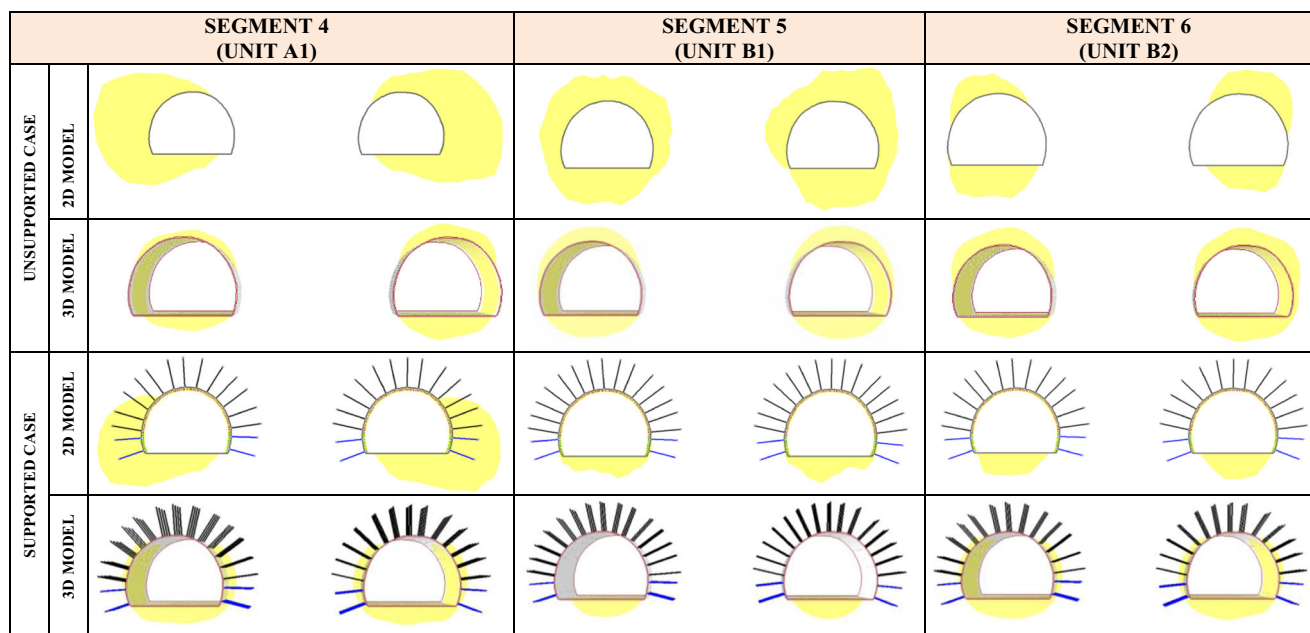


Fig. 10 2D and 3D numerical analyses showing the maximum total displacement developed in segments 4, 5 and 6 for the unsupported and supported cases

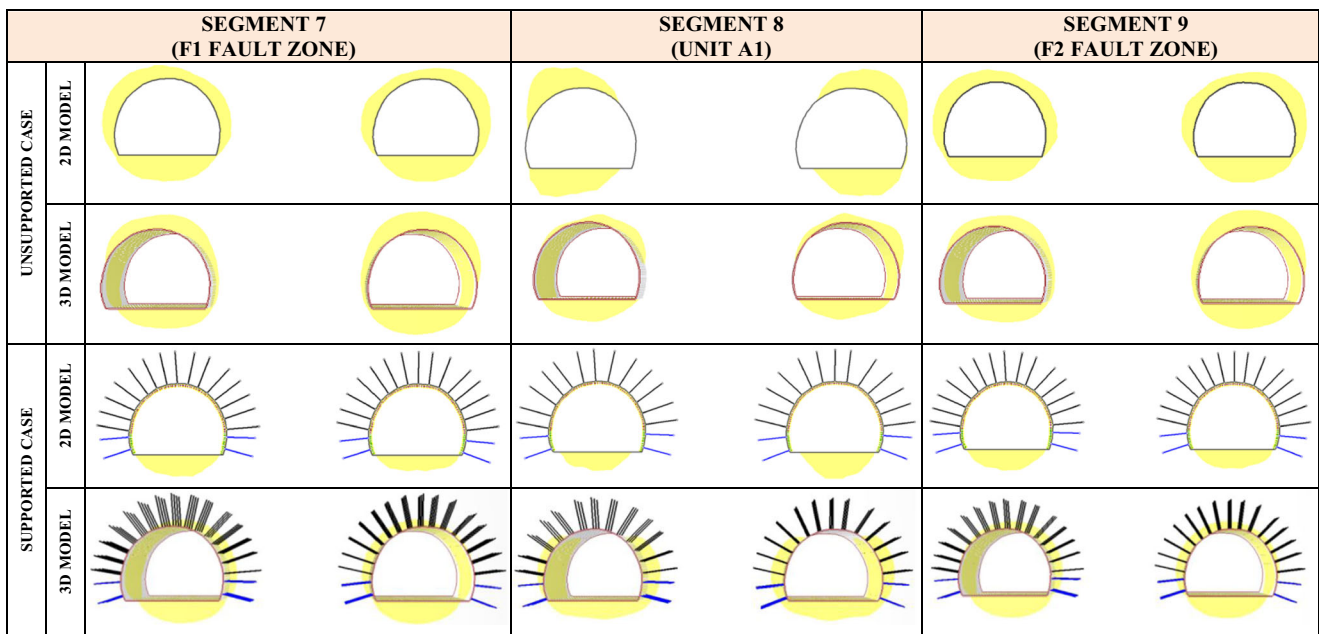


Fig. 11 2D and 3D numerical analyses showing the maximum total displacement developed in segments 7, 8 and 9 for the unsupported and supported cases

models, it was seen that the failure areas are in the zone of the assembled bolts for all tunnel parts except these segments. Therefore, it was suggested to use rock bolts longer than 4 m at the level of the crown in segments 4, 6 and 8.

The 2D and 3D numerical analyses have become the most chosen ones in underground applications by many researchers. Dhawan et al. (2002) revealed that the 2D

elasto-plastic tunnel analysis underestimates the deformations. On the other hand, it was determined that the 3D elasto-plastic analysis yields results which compare reasonably well with the in situ measurements. Ucer (2006) noted that the deformation analyses results of the 3D analyses in tunneling are in good agreement with the site data compared to the 2D analyses. Trinh et al. (2010) indicated that the 3D model is a much

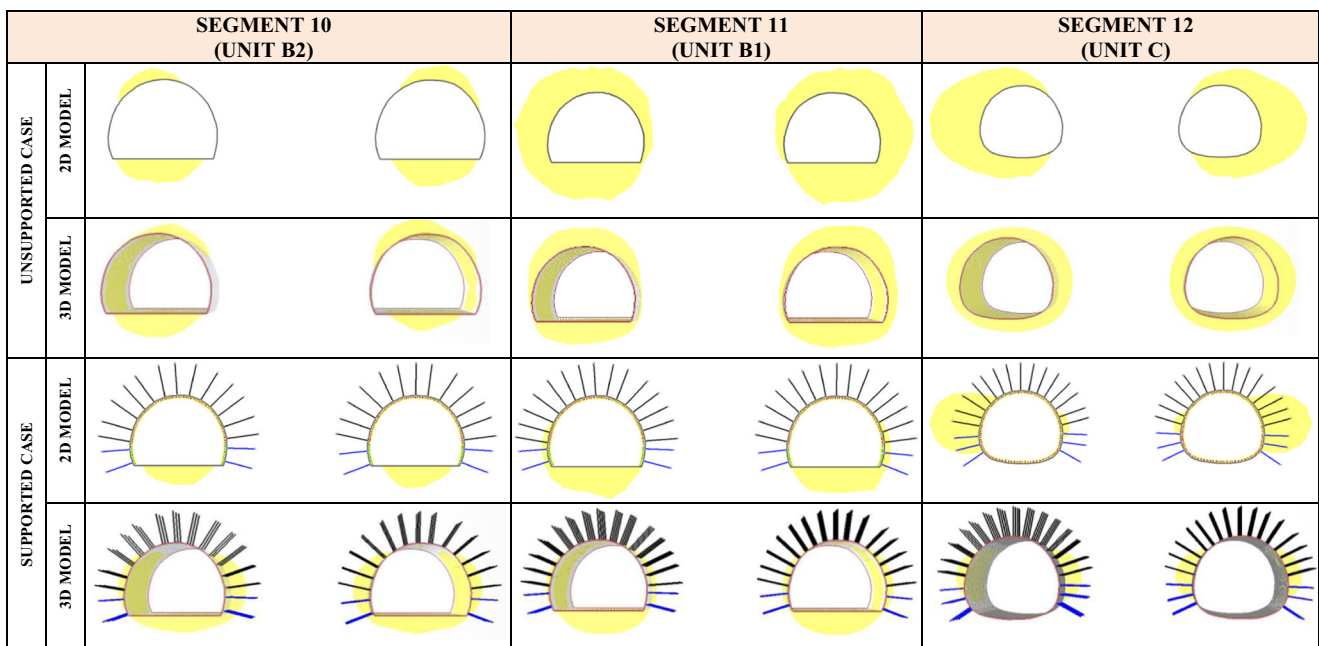


Fig. 12 2D and 3D numerical analyses showing the maximum total displacement developed in segments 10, 11 and 12 for the unsupported and supported cases

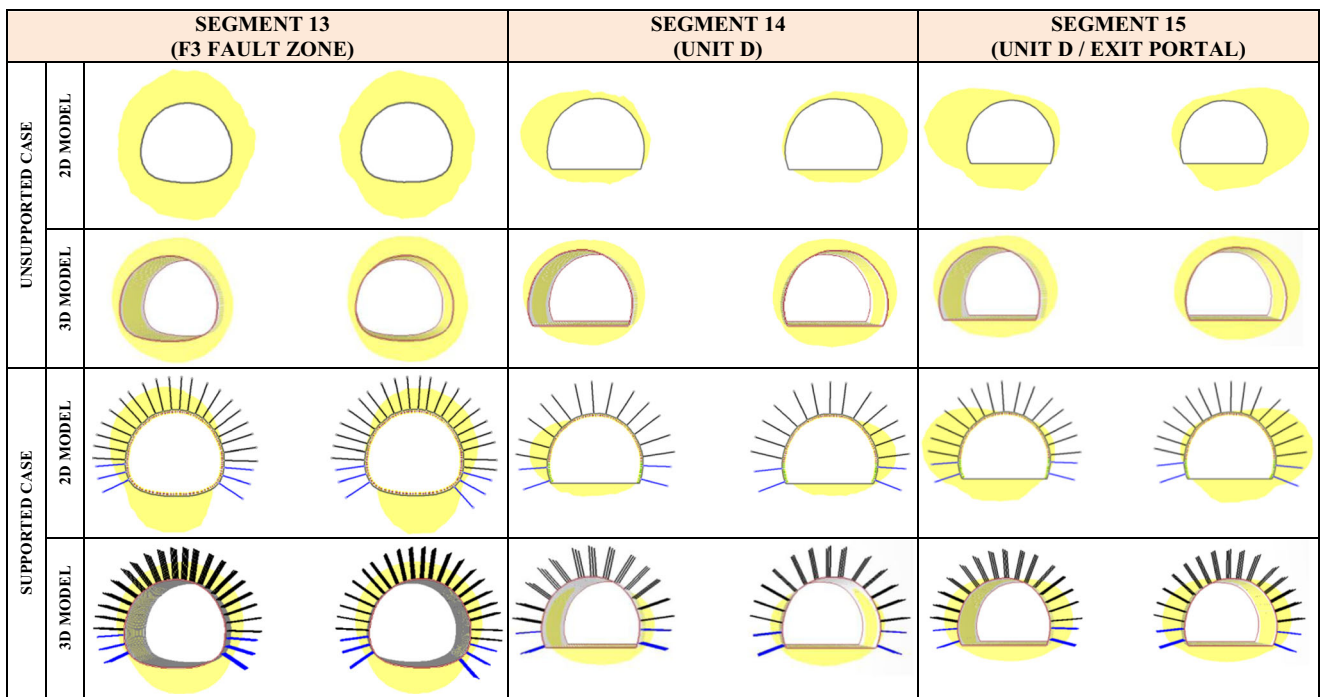


Fig. 13 2D and 3D numerical analyses showing the maximum total displacement developed in segments 13, 14 and 15 for the unsupported and supported cases

more powerful tool than 2D model in stress and strain estimations. Xu et al. (2015) noted that the precision of the 3D design is larger than that of the 2D prediction models. Furthermore, it was indicated that the 3D estimation models are required for absolute prediction owing to their higher accuracy and applicability in a wider range of complex

practical problems. Kaya and Sayin (2017) reported that the 3D FEM model presents the best remedy in lining pattern compared to 2D models. It is clearly seen that the findings of the present study exactly coincide with the results of research mentioned above. According to results of the 2D models under great in situ rock stresses, the over-estimated

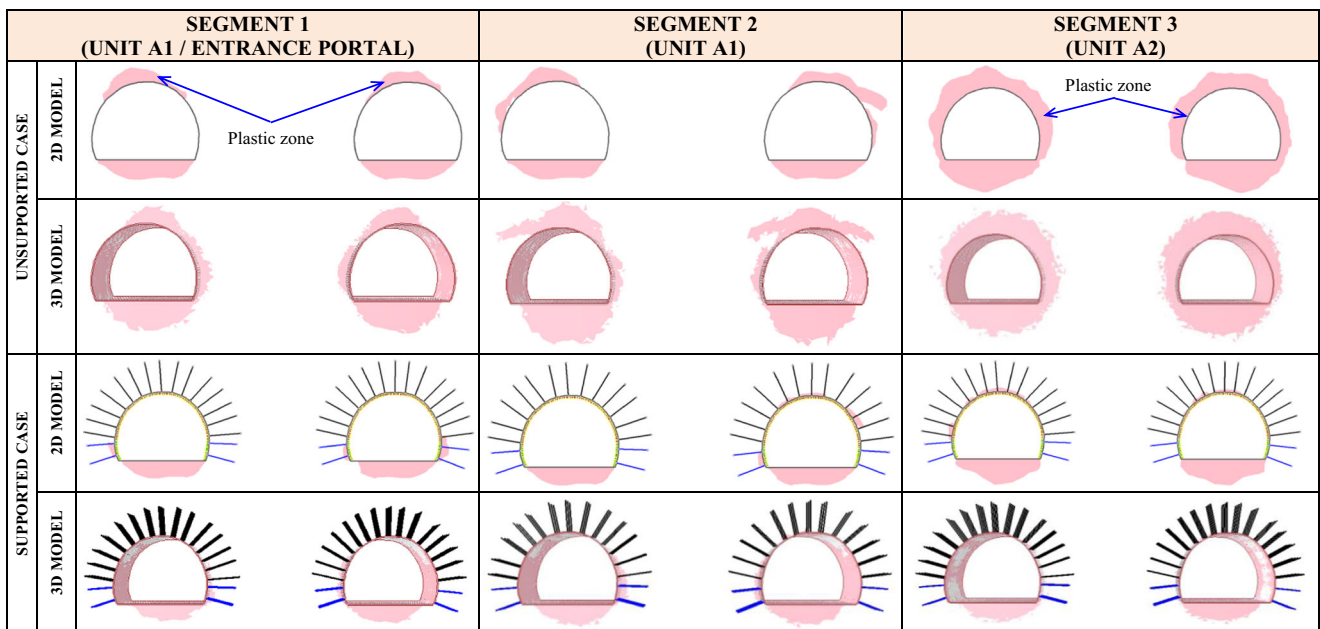


Fig. 14 2D and 3D numerical analyses showing the plastic zones developed in segments 1, 2 and 3 for the unsupported and supported cases

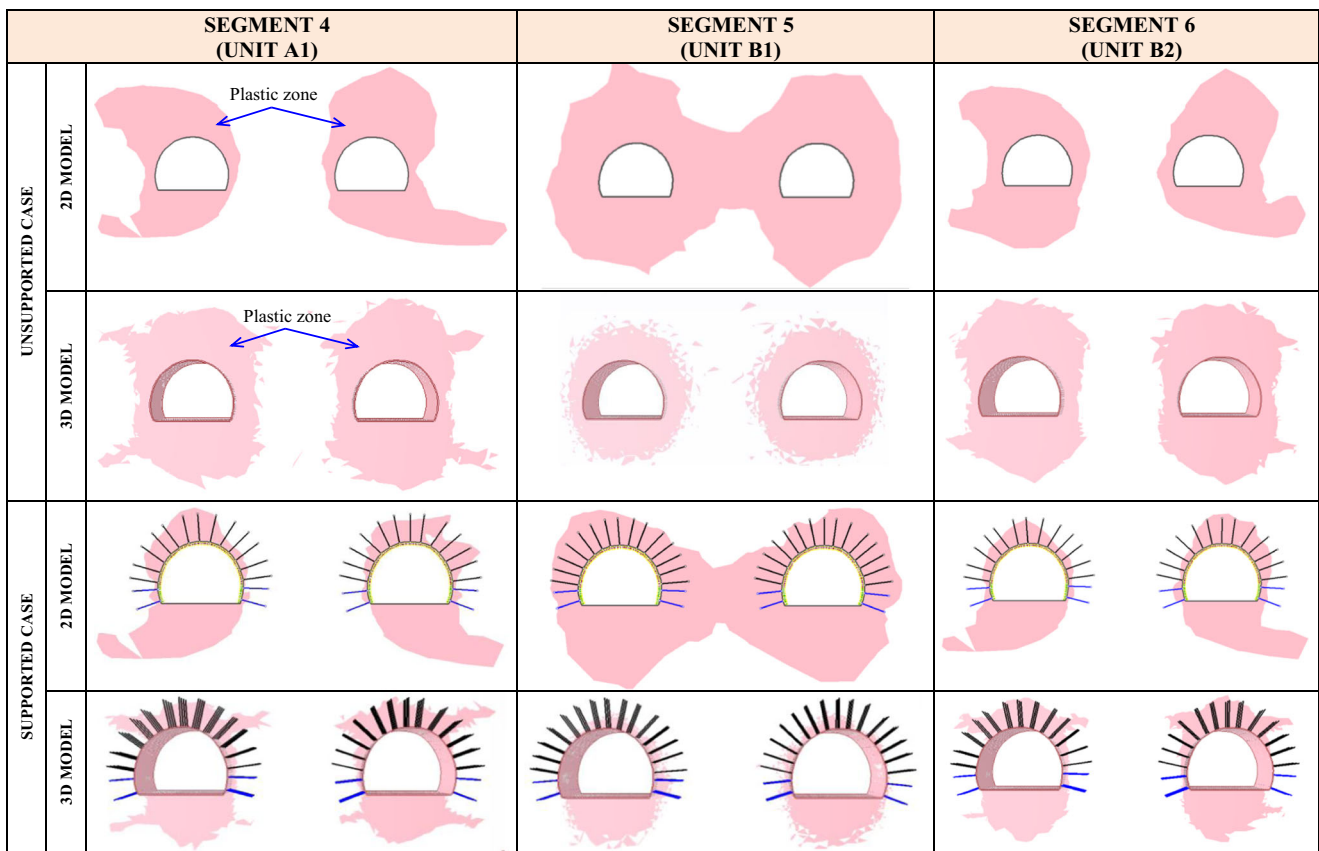


Fig. 15 2D and 3D numerical analyses showing the plastic zones developed in segments 4, 5 and 6 for the unsupported and supported cases

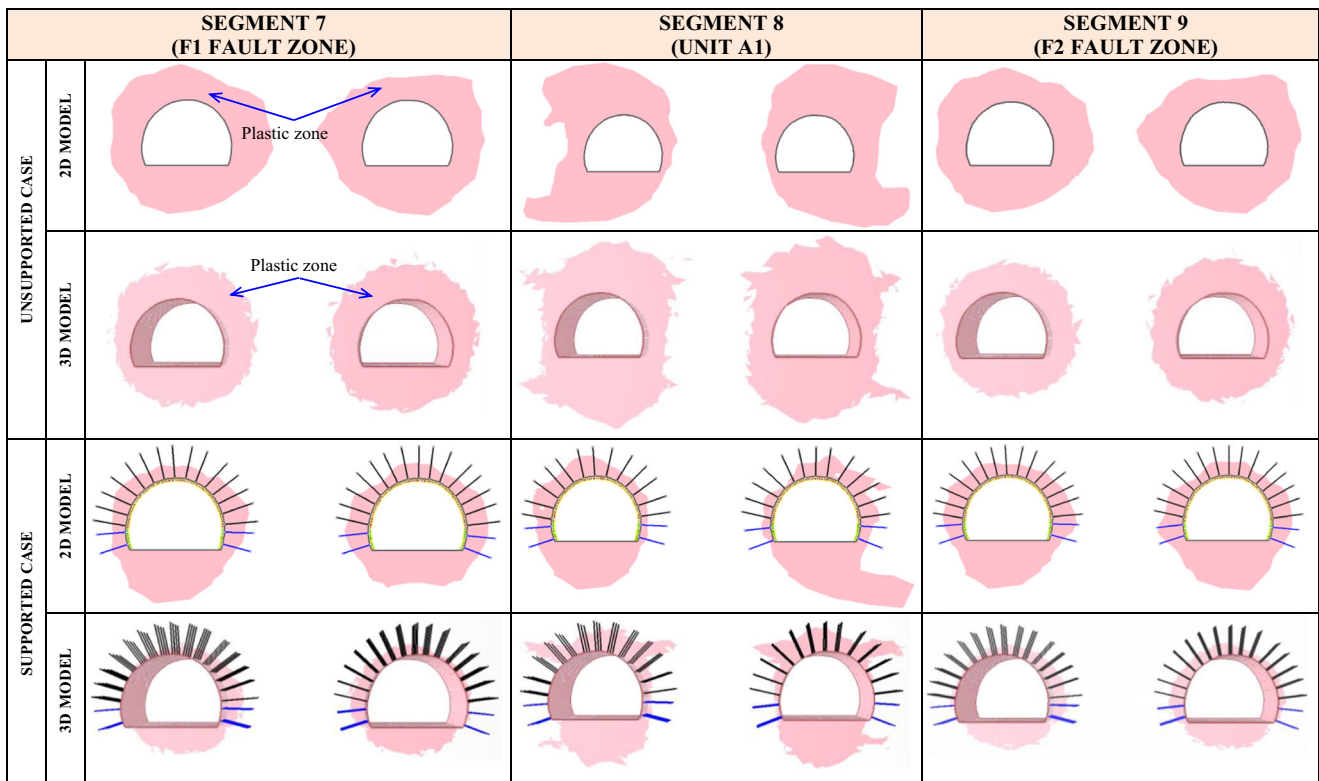


Fig. 16 2D and 3D numerical analyses showing the plastic zones developed in segments 7, 8 and 9 for the unsupported and supported cases

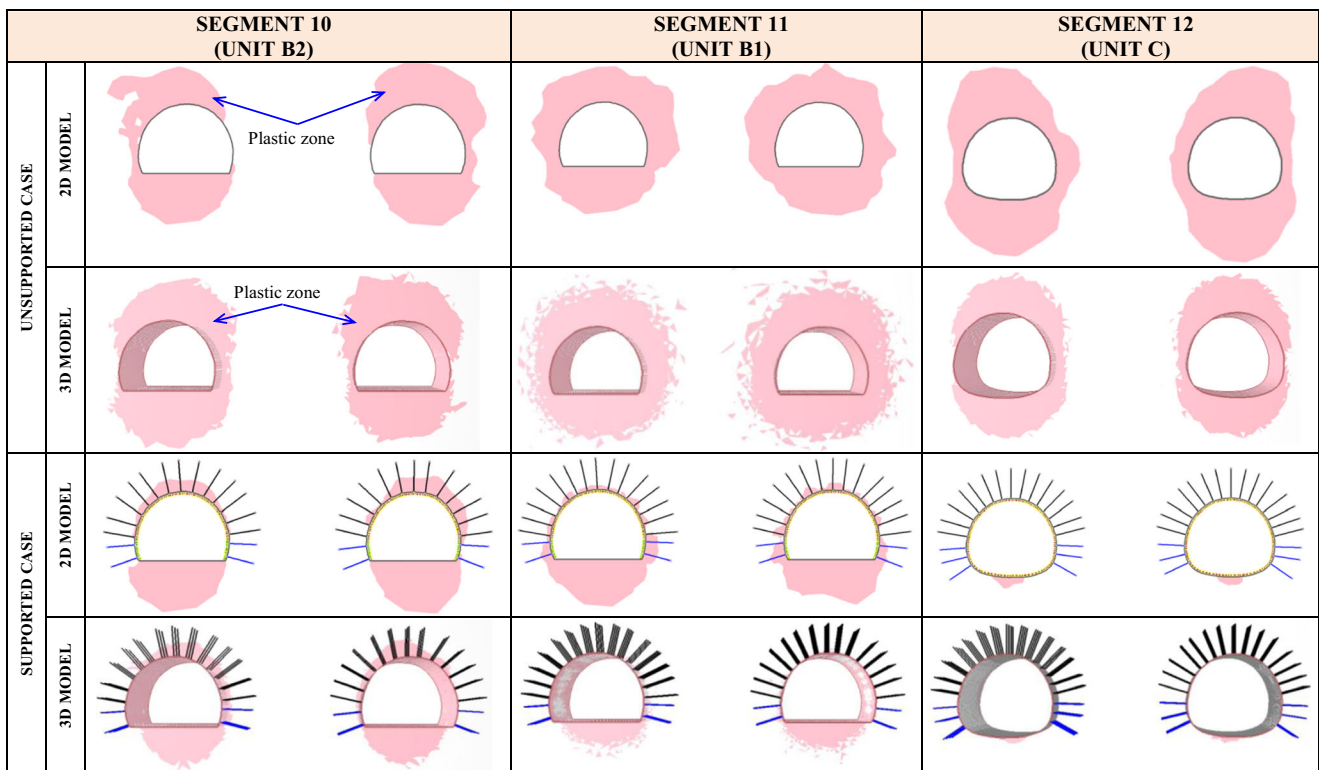


Fig. 17 2D and 3D numerical analyses showing the plastic zones developed in segments 10, 11 and 12 for the unsupported and supported cases

displacements and plastic zones were obtained compared to the 3D models. Therefore, the utilization of 3D modeling in design of the tunneling seems to be safe.

Consequently, the outcomes of the CC method in all matters depending on the deformational behavior and performance of the empirical lining were not in good agreement

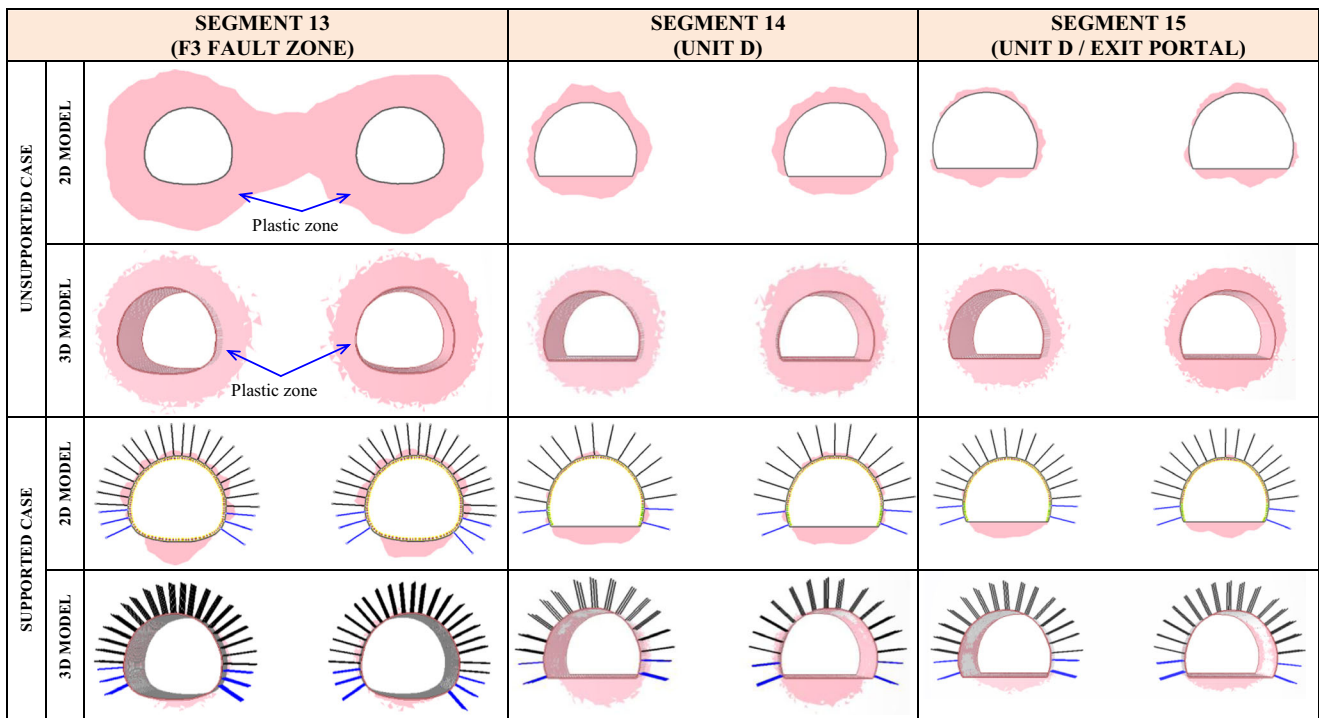


Fig. 18 2D and 3D numerical analyses showing the plastic zones developed in segments 13, 14 and 15 for the unsupported and supported case

with the related outputs of the FEM-based 2D and 3D models. However, as checked against to the 2D method, the 3D model may be very advantageous for tunnel engineers to define the safety in a more accurate way.

Conclusions

In the present study, the stability evaluation and the lining design of the Cankurtaran Tunnel, which is built in Artvin City (Turkey), was researched. Considering the data compiled from field and laboratory investigations, the quality of the tunnel ground segments were defined by the help of the RMR and Q systems as ranging from extremely poor to fair. After the application of the rock mass classifications, the four empirical lining design classes and the essential engineering geological characteristic properties forming the tunnel ground were obtained.

The applicability of the empirically determined support element was firstly controlled by the help of the convergence-confinement (CC) technique. Interaction between rock masses and tunnel support was also investigated analytically. According to the acquired results, the empirical lining design was only satisfactory for segments 1, 2, 3, 10, 12, 14 and 15. Except for these segments, it was concluded that the proposed lining designs are not successful to prevent the stability problem owing to the great field stresses.

In addition to the CC analysis, the FEM-based 2D and 3D software programs were utilized to check the efficiency of the empirical lining, and to numerically define the plastic zones and convergences that occurred around the ground surrounding the tunnel. Following application of the lining support, the size of the plastic zones around the opening was ordinarily decreased. Thus, it was determined that the empirical lining suggestions given for the Cankurtaran Tunnel project were generally acceptable. Support systems have been accomplished in suppressing the thickness of the plastic zone occurring around the tunnel excavation. However, it was determined that there are still plastic zones at the level of the tunnel roof in segments 4, 6 and 8. Application of rock bolts longer than 4 m was suggested for these zones. The results of the numerical analyses indicated that the most unsuitable deformation and the load scenario on lining elements are within admissible limits, and that the empirical support designs are considered to be reliable enough to support the excavation. Finally, it was concluded that the 3D FEM modelling presents the best answer in lining design compared to the CC method and 2D FEM analysis.

As an important addition of future studies on this topic, it is recommended that the in situ monitoring data should be taken throughout the construction stage of the excavation for adjustment of the FEM designs and for checking the accuracy of the suggested lining support.

Acknowledgements The authors would like to acknowledge to the editor and reviewers for their valuable contribution. Also, thanks to MSc. Geology Engineer Aytuna Sayin from the Turkish General Directorate of Highways (TGDH) for the office work associated with this study.

References

- Aydan O, Akagi T, Kawamoto T (1993) The squeezing potential of rocks around tunnels; theory and prediction. *Rock Mech Rock Eng* 26(2): 137–163
- Aydan O, Ulusay R, Kawamoto T (1997) Assessment of rock mass strength for underground excavations, proceedings of the 36th US rock mechanics symposium, New York, pp 777–786
- Aydan O, Ulusay R, Tokashiki N (2014) A new rock mass quality rating system: rock mass quality rating (RMQR) and its application to the estimation of geomechanical characteristics of rock masses. *Rock Mech and Rock Eng* 47(4):1255–1276
- Aydin A, Ozbek A, Acar A (2014) Geomechanical characterization, 3-D optical monitoring and numerical modeling in Kirkgecit-1 tunnel, Turkey. *Eng Geol* 181:38–47
- Barton NR (2002) Some new Q-value correlations to assist in site characterization and tunnel design. *Int J Rock Mech Min Sci* 39:185–216
- Barton NR, Lien R, Lunde J (1974) Engineering classification of rock masses for the design of tunnel support. *Rock Mech* (4):189–239
- Basarir H (2006) Engineering geological studies and tunnel support design at Sulakyurt dam site, Turkey. *Eng Geol* 86:225–237
- Basarir H, Ozsan A, Karakus M (2005) Analysis of support requirements for a shallow diversion tunnel at Guledar dam site, Turkey. *Eng Geol* 81(2):131–145
- Bieniawski ZT (1974) Geomechanics classification of rock masses and its application in tunneling, Proceedings of the Third International Congress on Rock Mechanics, Vol. 1A. International Society of Rock Mechanics, Denver, 27–32
- Bieniawski ZT (1989) Engineering rock mass classifications. Wiley, New York, p 251
- Cai M, Kaiser PK, Tasaka Y, Minami M (2007) Determination of residual strength parameters of jointed rock masses using the GSI system. *Int J Rock Mech Min Sci* 4(2):247–265
- Capkinoglu S (1981) Geology of the district between Borcka and Cavuslu (Hopa), MSc. thesis, Karadeniz Technical University, Trabzon, Turkey
- Carranza-Torres C, Engen M (2017) The support characteristic curve for blocked steel sets in the convergence-confinement method of tunnel support design. *Tun Und Space Tech* 69:233–244
- Carranza-Torres C, Fairhurst C (1999) The elasto-plastic response of underground excavations in rock masses that satisfy the Hoek–Brown failure criterion. *Int J Rock Mech Min Sci* 36(6):777–809
- Carranza-Torres C, Fairhurst C (2000) Application of the convergence-confinement method of tunnel design to rock-masses that satisfy the Hoek–Brown failure criterion. *Tun. Und. Space Tech.* 15(2):187–213
- Curran JH, Hammah RE, Thamer EY (2003) A two dimensional approach for designing tunnel support in weak rock, Proc. 56th Canadian Geotech. Conference, Winnepeg, Monibota
- Deere DU (1964) Technical description of rock cores for engineering purposed. *Rock Mech Rock Eng* 1:17–22
- Dhawan KR, Singh DN, Gupta ID (2002) 2D and 3D finite element analysis of underground openings in an inhomogeneous rock mass. *Int J Rock Mech Min Sci* 39:217–227
- Genis M, Basarir H, Ozarslan A, Bilir E, Balaban E (2007) Engineering geological appraisal of the rockmasses and preliminary support design, Dorukhan tunnel, Zonguldak, Turkey. *Eng Geol* 92:14–26

- Gurocak Z, Solanki P, Zaman MM (2007) Empirical and numerical analyses of support requirements for a diversion tunnel at the Boztepe dam site, eastern Turkey. *Eng Geol* 91:194–208
- Guven IH (1993) 1:250000-scaled geology and compilation of the Eastern Pontide. General Directorate of Mineral Research and Exploration (MTA) of Turkey, Ankara (unpublished)
- Hoek E (2007) Practical Rock Engineering, Evert Hoek Consulting Engineer Inc., Vancouver, Canada (Available for download at), <https://www.rocsience.com/learning/hoek-s-corner/books>
- Hoek E, Diederichs MS (2006) Empirical estimation of rock mass modulus. *Int J Rock Mech Min Sci* 43:203–215
- Hoek E, Marinos P (2000) Predicting tunnel squeezing. *Tunnels and Tunneling International*, Part 1 – November 2000, Part 2–December 2000
- Hoek E, Kaiser PK, Bawden WF (1995) Support of underground excavations in hard rock. AA Balkema, Rotterdam
- Hoek E, Carranza-Torres C, Corkum B (2002) Hoek-Brown failure criterion-2002 edition. proceedings of NARMS-TAC2002, mining innovation and technology. Toronto, Canada, pp 267–273
- ISRM (2007) The complete ISRM suggested methods for rock characterization, testing and monitoring: 1974–2006, International Society of Rock Mechanics Turkish National Group, Ankara, Turkey, 628
- Javadi AA, Snee CPM (2002) Numerical modeling of air losses in compressed air tunneling. *Int J Geomech* 2(4):399–417
- Kanik M, Gurocak Z (2018) Importance of numerical analyses for determining support systems in tunneling: a comparative study from the Trabzon-Gumushane tunnel, Turkey. *J Afr Earth Sci* 143:253–265
- Kanik M, Gurocak Z, Alemdag S (2015) A comparison of support systems obtained from the RMR₉₉ and RMR₁₄ by numerical analyses: Macka tunnel project, NE Turkey. *J Afr Ear Sci* 109:224–238
- Kaya A, Sayin A (2017) Engineering geological appraisal and preliminary support design for the Salarha tunnel, Northeast Turkey. *Bul Eng Geo Env*. <https://doi.org/10.1007/s10064-017-1177-2>
- Kaya A, Bulut F, Alemdag S, Sayin A (2011) Analysis of support requirements for a tunnel portal in weak rock: a case study in Turkey. *Sci Res Ess* 6(31):6566–6583
- Ketin I (1966) Tectonic units of Anatolia. *J Gen Direc Min Res Exp*, (MTA) 66:23–34
- Kockar MK, Akgun H (2003) Engineering geological investigations along the Iliku tunnels, southern Turkey. *Eng Geol* 68(3–4):141–158
- Lauffer H (1958) Classification of in-situ rock in tunnel construction. *Geology Bauwesen* 24:46–51
- Lin SY, Hung HH, Yang JP, Yang YB (2017) Seismic analysis of twin tunnels by a finite/infinite element approach. *Int. J. Geomech*. [https://doi.org/10.1061/\(ASCE\)GM.1943-5622.0000677](https://doi.org/10.1061/(ASCE)GM.1943-5622.0000677)
- Lugeon M (1933) Barrages et geologic methods de recherche´ terrassement et un permeabilisation. Litrairedes Universite, Paris
- Marinos P, Hoek E, (2000) GSI: a geologically friendly tool for rock mass strength estimation. In: Proceedings of the GeoEng2000 at the international conference on geotechnical and geological engineering, Melbourne, Technomic publishers, Lancaster, 1422–1446
- Ozdogan MV, Yenice H, Gonen A, Karakus D (2018) Optimal support spacing for steel sets: Omerler underground coal mine in western Turkey. *Int. J. Geomech*. [https://doi.org/10.1061/\(ASCE\)GM.1943-5622.0001069](https://doi.org/10.1061/(ASCE)GM.1943-5622.0001069)
- Ozsan A, Basarir H (2003) Support capacity estimation of a diversion tunnel in weak rock. *Eng Geol* 68:319–331
- Ozsan A, Karpuz C (2001) Preliminary support design for Ankara subway extension tunnel. *Eng Geol* 59(1–2):161–172
- Palmström A (1995) RMI-a rock mass characterization system for rock engineering purposes, Ph.D. thesis, University of Oslo, Norway, 400
- Park KH (2004) Elastic solution for tunneling-induced ground movements in clays. *Int. J. Geomech*. 4:310–318
- Priest SD, Hudson JA (1976) Discontinuity spacing in rock. *Int J Rock Mech Min Sci Geo Abs* 13:135–148
- Quinones-Rozo C (2010) Lugeon test interpretation, revisited, In: Collaborative Management of Integrated Watersheds, 30rd Annual USSD (United States Society on Dams) Conference, US Society on Dams, Denver, CO, USA, 405–414
- Rabcewicz L (1964) The new Austrian Tunnelling method. *Water Power* 16:453–457
- Rocscience Inc (2016a) Dips v7.0 graphical and statistical analysis of orientation data, Toronto, Ontario, Canada, www.rocsience.com
- Rocscience Inc (2016b) RocData v5.0 rock, soil and discontinuity strength analysis, Toronto, Ontario, Canada, www.rocsience.com
- Rocscience Inc (2016c) RS³ v1.0 3D finite element analysis for rock and soil, Toronto, Ontario, Canada, www.rocsience.com
- Rocscience Inc. (2017) RS² v9.0 finite element analysis for excavations and slopes, Toronto, Ontario, Canada, www.rocsience.com
- Sari D, Pasamehmetoglu AG (2004) Proposed support design, Kaletepe tunnel, Turkey. *Eng Geol* 72:201–216
- Sheorey PR, Murali MG, Sinha A (2001) Influence of elastic constants on the horizontal in situ stress. *Int J Rock Mech Min Sci* 38(1):1211–1216
- Sopaci E, Akgun H (2008) Engineering geological investigations and the preliminary support design for the proposed Ordu peripheral highway tunnel, Ordu, Turkey. *Eng Geo* 96:43–61
- Terzaghi K (1946) Rock defects and loads on tunnel supports, in Proctor, R.V., and White, T.L., eds., *Rock tunneling with steel support*, Youngstown, Ohio, Commercial Shearing and Stamping Company, 1:17–99
- TGDH (2013) Specification for highway works (in Turkish), Turkish Ministry of Public Works, General Directorate of Highways, Ankara
- Trinh QN, Broch E, Lu M (2010) 2D versus 3D modeling for tunneling at a weakness zone, ISRM Regional Symposium-EUROCK 2009, Croatia
- Ucer S (2006) Comparison of 2D and 3D finite element models of tunnel advance in soft ground: A case study on Bolu tunnels, MSc Thesis, Middle East Technical University, Ankara, Turkey
- Wickham GE, Tiedemann HR, Skinner EH (1972) Support determination based on geologic predictions, In: Lane, K.S.A.G., L. A., ed., *North American Rapid Excavation and Tunneling Conference*: Chicago, New York: Society of Mining Engineers of the American Institute of Mining, Metallurgical and Petroleum Engineers, 43–64
- Wyllie DC, Mah CW (2004) *Rock slope engineering civil and mining*, Spon Press, Taylor and Francis e-library
- Xu Q, Xiao Z, Liu T, Lou T, Song X (2015) Comparison of 2D and 3D prediction models for environmental vibration induced by underground railway with two types of tracks. *Comput Geotech* 68: 169–183
- Yalcin E, Gurocak Z, Ghabchi R, Zaman M (2015) Numerical analysis for a realistic support design: case study of the Komurhan tunnel in eastern Turkey. *Int. J. Geomech*. [https://doi.org/10.1061/\(ASCE\)GM.1943-5622.0000564](https://doi.org/10.1061/(ASCE)GM.1943-5622.0000564)